AMERICAN SOCIETY FOR MICROBIOLOGY | mBio®

RESEARCH ARTICLE

Toxoplasma gondii GRA28 Is Required for Placenta-Specific Induction of the Regulatory Chemokine CCL22 in Human and Mouse

Elizabeth N. Rudzki,[a] Stephanie E. Ander,[a,b] Rachel S. Coombs,[a] Hisham S. Alrubaye,[a] Leah F. Cabo,[a] Matthew L. Blank,[a] Nicolás Gutiérrez-Melo,[a] J. P. Dubey,[c] Carolyn B. Coyne,[d] Jon P. Boyle[a]

[a]Department of Biological Sciences, Dietrich School of Arts and Sciences, University of Pittsburgh, Pittsburgh, Pennsylvania, USA
[b]Department of Pediatrics, University of Pittsburgh School of Medicine, Pittsburgh, Pennsylvania, USA
[c]Animal Parasitic Diseases Laboratory, Beltsville Agricultural Research Center, Agricultural Research Service, U.S. Department of Agriculture, Beltsville, Maryland, USA
[d]Department of Molecular Genetics and Microbiology, Duke University School of Medicine, Durham, North Carolina, USA

ABSTRACT *Toxoplasma gondii* is an intracellular protozoan pathogen of humans that can cross the placenta and result in adverse pregnancy outcomes and long-term birth defects. The mechanisms used by *T. gondii* to cross the placenta are unknown, but complex interactions with the host immune response are likely to play a role in dictating infection outcomes during pregnancy. Prior work showed that *T. gondii* infection dramatically and specifically increases the secretion of the immunomodulatory chemokine CCL22 in human placental cells during infection. Given the important role of this chemokine during pregnancy, we hypothesized that CCL22 induction was driven by a specific *T. gondii*-secreted effector. Using a combination of bioinformatics and molecular genetics, we have now identified *T. gondii* GRA28 as the gene product required for CCL22 induction. GRA28 is secreted into the host cell, where it localizes to the nucleus, and deletion of the GRA28 gene results in reduced CCL22 placental cells as well as a human monocyte cell line. The impact of GRA28 on CCL22 production is also conserved in mouse immune and placental cells both *in vitro* and *in vivo*. Moreover, parasites lacking GRA28 are impaired in their ability to disseminate throughout the animal, suggesting a link between CCL22 induction and the ability of the parasite to cause disease. Overall, these data demonstrate a clear function for GRA28 in altering the immunomodulatory landscape during infection of both placental and peripheral immune cells and show a clear impact of this immunomodulation on infection outcome.

IMPORTANCE *Toxoplasma gondii* is a globally ubiquitous pathogen that can cause severe disease in HIV/AIDS patients and can also cross the placenta and infect the developing fetus. We have found that placental and immune cells infected with *T. gondii* secrete significant amounts of a chemokine (called CCL22) that is critical for immune tolerance during pregnancy. In order to better understand whether this is a response by the host or a process that is driven by the parasite, we have identified a *T. gondii* gene that is absolutely required to induce CCL22 production in human cells, indicating that CCL22 production is a process driven almost entirely by the parasite rather than the host. Consistent with its role in immune tolerance, we also found that *T. gondii* parasites lacking this gene are less able to proliferate and disseminate throughout the host. Taken together, these data illustrate a direct relationship between CCL22 levels in the infected host and a key parasite effector and provide an interesting example of how *T. gondii* can directly modulate host signaling pathways in order to facilitate its growth and dissemination.

KEYWORDS CCL22, *Toxoplasma gondii*, placenta, teratogenic, virulence

Toxoplasma gondii is an obligate intracellular parasite that is an important parasite of humans and other animals. While this pathogen is particularly well known to cause severe disease in the immunocompromised, such as those with HIV/AIDS or undergoing

Citation Rudzki EN, Ander SE, Coombs RS, Alrubaye HS, Cabo LF, Blank ML, Gutiérrez-Melo N, Dubey JP, Coyne CB, Boyle JP. 2021. *Toxoplasma gondii GRA28* is required for placenta-specific induction of the regulatory chemokine CCL22 in human and mouse. mBio 12:e01591-21. https://doi.org/10.1128/mBio.01591-21.

Editor Barbara Burleigh, Harvard T. H. Chan School of Public Health

Address correspondence to Jon P. Boyle, boylej@pitt.edu.

Received 3 June 2021
Accepted 17 September 2021
Published 16 November 2021

immunosuppression for organ transplants, *T. gondii* is also capable of crossing the placenta and infecting the developing fetus, leading to a variety of infection outcomes, ranging from asymptomatic to severe (1). Importantly, even children born without symptoms are at high risk for extensive health problems later in life, including ocular disease and neurological disorders (2, 3). To date, little is known about how *T. gondii* gains access to the fetal compartment and how the host responds to the presence of parasites at the maternal-fetal interface.

Recently, we (4) found that primary human trophoblast cells (derived from term placentas) and second trimester placental explants produced the chemokine CCL22 in response to infection with *T. gondii* (4). Production of this chemokine was dependent on parasite invasion and the dense granule effector trafficking gene product MYR1 (4). While the role of CCL22 during infection with *T. gondii* is poorly understood, this chemokine is a key molecular signal for the recruitment of regulatory T cells, which are well known for their role in suppressing immune responses to tumors, leading to poor clinical outcomes (5, 6). Importantly, disruption of T_{reg} recruitment to tumors can lead to improved outcomes in animal models. For example, using *Ccl22* DNA vaccines in mice leads to misdirection of regulatory T cells and ultimately reduced tumor growth (5). The role for CCL22 in healthy humans is less well understood, although it is thought to subvert and/or modulate inflammatory responses and may be particularly important for response resolution after pathogen clearance. CCL22 and regulatory T cells also play a critical role during pregnancy, where they seem to govern immune tolerance (7) and regulation of inflammation at the maternal-fetal interface. This regulatory role appears to be critical in determining pregnancy outcome during pathogen-mediated immune activation (7, 8). Given the important role played by CCL22 during pregnancy and our recent findings regarding the ability of a congenitally acquired parasite to directly modulate production of this chemokine, we sought to identify the parasite effector (s) responsible for this in order to determine the impact of CCL22 modulation on congenital transmission and pregnancy outcome during vertical transmission. To do this, we used a bioinformatic screen to identify candidate genes and identified one (*GRA28*; *TGGT1_231960*) as being required for CCL22 induction in human and mouse cells. Overall, these data show that a specific effector is largely responsible for *T. gondii*-mediated CCL22 induction in a relatively small number of human and mouse cell types and suggest that the manipulation of CCL22 levels by GRA28 may influence the ability of *T. gondii* to disseminate throughout the host.

RESULTS

***Toxoplasma gondii* induces a monocyte-like cell line to produce the immunomodulatory chemokine CCL22.** Previous work established that placental explants and primary human trophoblasts infected with *T. gondii* had increased *CCL22* transcript abundance and released more CCL22 protein into the culture medium than mock-infected controls (4). Since we also found that not all cell types produce CCL22 in response to infection (e.g., human foreskin fibroblasts [HFFs]), we were interested in identifying a human cell line that could be used as a more tractable model than placental cells to assay *T. gondii*-driven CCL22 induction. THP-1 cells, a cell line derived from a patient with monocytic leukemia, were a reasonable candidate given their origins in the myeloid lineage and known production of CCL22 in response to a variety of stimuli (9, 10). We infected THP-1 cells with a type 1 *T. gondii* strain (RH88 or RH*YFP* [4]) at a multiplicity of infection (MOI) of 3. Following 24 h of infection, supernatants were collected from each well. HFFs were infected in parallel as negative controls. Mock treatments involved passing the parasite solution through a 0.22-μm-pore-size filter prior to exposure to the cells. Based on a CCL22 ELISA, *T. gondii* infection induced CCL22 in THP-1 cells, and as expected there was no CCL22 production from mock-treated controls or *T. gondii*-infected HFFs (Fig. 1A). We also infected primary placental tissues in the same manner, and as expected, villous tree explants and decidua taken from second trimester placentas produced significantly more CCL22 than mock-treated controls (Fig. 1A). In addition to the type 1 RH strain, other *T. gondii* strain types (type 2, strain PRU, and type 3, strain CEP) (see Fig. S1A in the supplemental material) also induced secretion of CCL22 from THP-1 cells, as did the nearest extant relative of *T. gondii*, *Hammondia hammondi* (Fig. S1B). In contrast to *H. hammondi*,

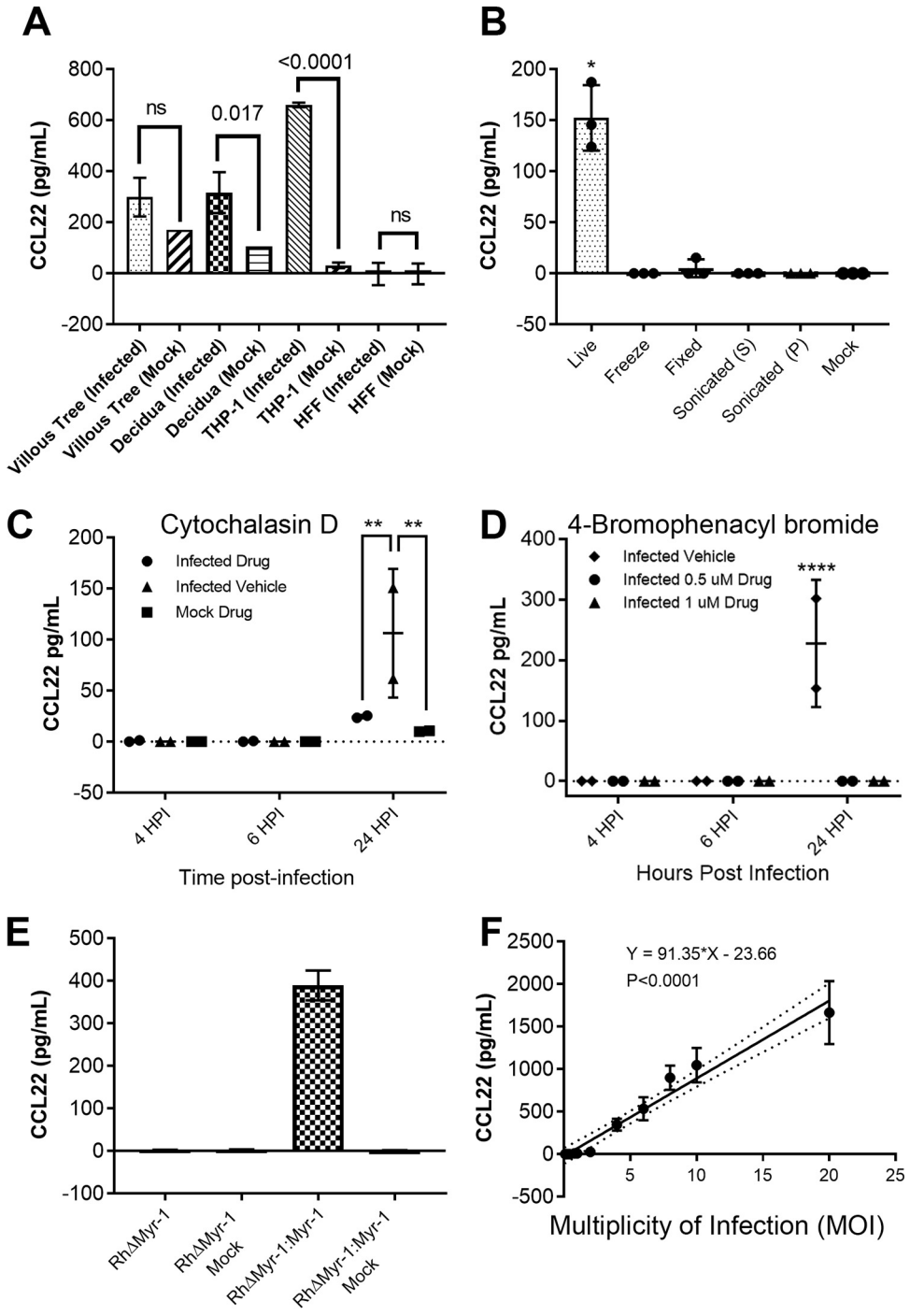

FIG 1 (A) THP-1 cells, human foreskin fibroblasts (HFFs), and second trimester placental samples of villous trees and decidual tissue were infected with a type 1 strain of *Toxoplasma gondii* (RH:YFP). Statistics on the THP-1 cell and HFF cell samples were performed by ordinary two-way ANOVA with Tukey's multiple-comparison test. Statistics on the placental samples were performed by two-tailed Welch-corrected *t* tests. (B) Type 1 strain (RH) *T. gondii* parasites were subjected to multiple treatments as described in Materials and Methods. The soluble fraction of the sonicated treatment is denoted by S; the insoluble fraction is denoted by P. THP-1 cells were then exposed to either live parasites or treated parasites. Statistics were performed by multiple two-tailed Welch-corrected *t* test comparisons with the live parasite treatment at a *P* of ≤0.0145. (C and D) Type 1 strain (RH) *T. gondii* parasites were treated with either cytochalasin D (C) or 4-bromophenacyl bromide (D) as described in Materials and Methods. THP-1 cells were then infected with the respective parasite treatment. Statistics were performed by two-way ANOVA and multiple-comparison *post hoc* tests, where the Cyt-D *P* value is 0.009, and the 4-BPB *P* value is <0.0001. (E) Type 1 strain (RH) *T. gondii* parasites deficient in Myr-1 (TgRHΔ*Myr-1*) and their complement (TgRHΔ*Myr-1:Myr-1*$_c$) were used to infect THP-1 cells. (F) Type 1 strain (RH) *T. gondii* parasites were used to infect THP-1 cells at MOIs of 20, 10, 8, 6, 4, 3, 1, 0.8, 0.4, 0.2, and 0.1. (A to D) The respective cells/tissues were infected at a multiplicity of infection (MOI) of 3. Supernatants were collected at 24 h postinfection unless indicated otherwise and assayed by CCL22 ELISA.

and just as we observed previously in primary human placental cells (4), *Neospora caninum* had no effect on THP-1 production of CCL22 (Fig. S1B). These data provided strong support that the mechanism of CCL22 induction is the same for THP-1 and placental cells.

We also determined if live parasites were required to induce CCL22 in THP-1 cells by exposing host cells to parasites that were exposed to a variety of lethal treatments. As shown in Fig. 1B, dead parasites failed to induce CCL22 production by THP-1 cells. We also pretreated parasites and host cells with 10 μg/ml cytochalasin D (Cyt-D) to block invasion (11), and as shown in Fig. 1C, Cyt-D-treated parasites were significantly impaired in their ability to induce CCL22, suggesting that active invasion was required for this phenomenon. We obtained similar results with the inhibitor 4-bromophenacyl bromide (4-BPB) (Fig. 1D), which also significantly blocked CCL22 production by THP-1 cells at 0.5 and 1 μM. This drug blocks rhoptry and dense granule secretion from *T. gondii* but not microneme secretion (12), suggesting that the factor is not a microneme protein (Fig. 1D). We also infected THP-1 cells with *T. gondii* parasites that were deficient in the dense granule trafficking protein MYR1 (13) (kind gift from John Boothroyd, Stanford University) and compared them to *T. gondii* RHΔ*MYR1*:*MYR1*$_c$ (TgRHΔ*MYR1*:*MYR1*$_c$) parasites. TgRHΔ*MYR1* parasites failed to induce any detectable CCL22 from THP-1 cells, while, as expected, TgRHΔ*MYR1*:*MYR1*$_c$ parasites induced significantly more than mock-treated cells (Fig. 1E). We also observed a very tight correlation between parasite multiplicity of infection (MOI) and CCL22 levels, suggesting that the signal was driven primarily by the parasite rather than the host cell (Fig. 1F). Based on these results, we felt confident that the unknown secreted factor driving CCL22 production in human primary placental cells was very likely the same as the one driving it in the THP-1 cell line and chose THP-1 cells for screening candidate effectors given their tractability in the laboratory.

Transcript abundance correlation analysis identifies a large group of putatively MYR1-trafficked gene products. As described previously (above and in reference 4), we have determined that primary human trophoblast cells infected with *T. gondii* have a transcriptional signature that is characterized by the production of immunomodulatory chemokines, with CCL22 being the most potently induced. To identify candidate *T. gondii* genes responsible for this effect on placental cells, and since this effect required the *T. gondii* effector translocation complex protein MYR1 (4), we hypothesized that MYR1-dependent substrates would have highly correlated gene expression profiles across diverse gene expression data sets. To test this hypothesis, we generated an "all versus all" correlation matrix of 396 *T. gondii* Affymetrix microarray data sets that we downloaded and curated from the Gene Expression Omnibus (see Materials and Methods). Analysis of the entire correlation matrix (shown in Fig. 2A and downloadable at https://doi.org/10.6084/m9.figshare.16451832) confirms this hypothesis for certain gene classes. For example, we identified one cluster containing multiple SAG-related sequences (SRS) which are typically expressed at high levels in bradyzoites (including SRS49 cluster members A, C, and D) (Fig. S2A) and another containing 70 genes, 43 of which encode ribosomal subunits (Fig. S2A). Examination of the gene expression heat maps across all 396 microarray analyses clearly show distinct patterns of gene expression in these two clusters depending on life stage treatment exposure (Fig. S2A and B).

We quantified the degree of transcript abundance correlation between 5 "bait" genes (*MYR1*, *MYR2*, and *MYR3* [13, 14] and the known *MYR1*-dependent substrates TgGRA24 and TgIST [15, 16]) and all other genes across all 396 expression data sets. We identified genes as candidate MYR1 substrates if they had an average correlation with the 5 "bait" genes of $\geq$0.7, a *dN*/*dS* ratio of $\geq$2, and the presence of a predicted signal peptide or at least one transmembrane domain. Using this set of filters, we were left with 28 candidate genes (plus all 5 bait genes, which also met these cutoffs), including the known TgMYR-dependent substrate TgGRA25 (17). Since all known MYR1 trafficked substrates are dense granule proteins, we eliminated any surface antigens or soluble enzymes, leaving a number of confirmed dense granule proteins (e.g., GRA4 and GRA8) and conserved hypothetical proteins. Importantly, when we examined the correlation between the bait genes and all *T. gondii* genes annotated as "dense granule" either in the primary product notes or via user annotation, we found that not all dense granule-encoding transcripts correlated highly with bait transcript

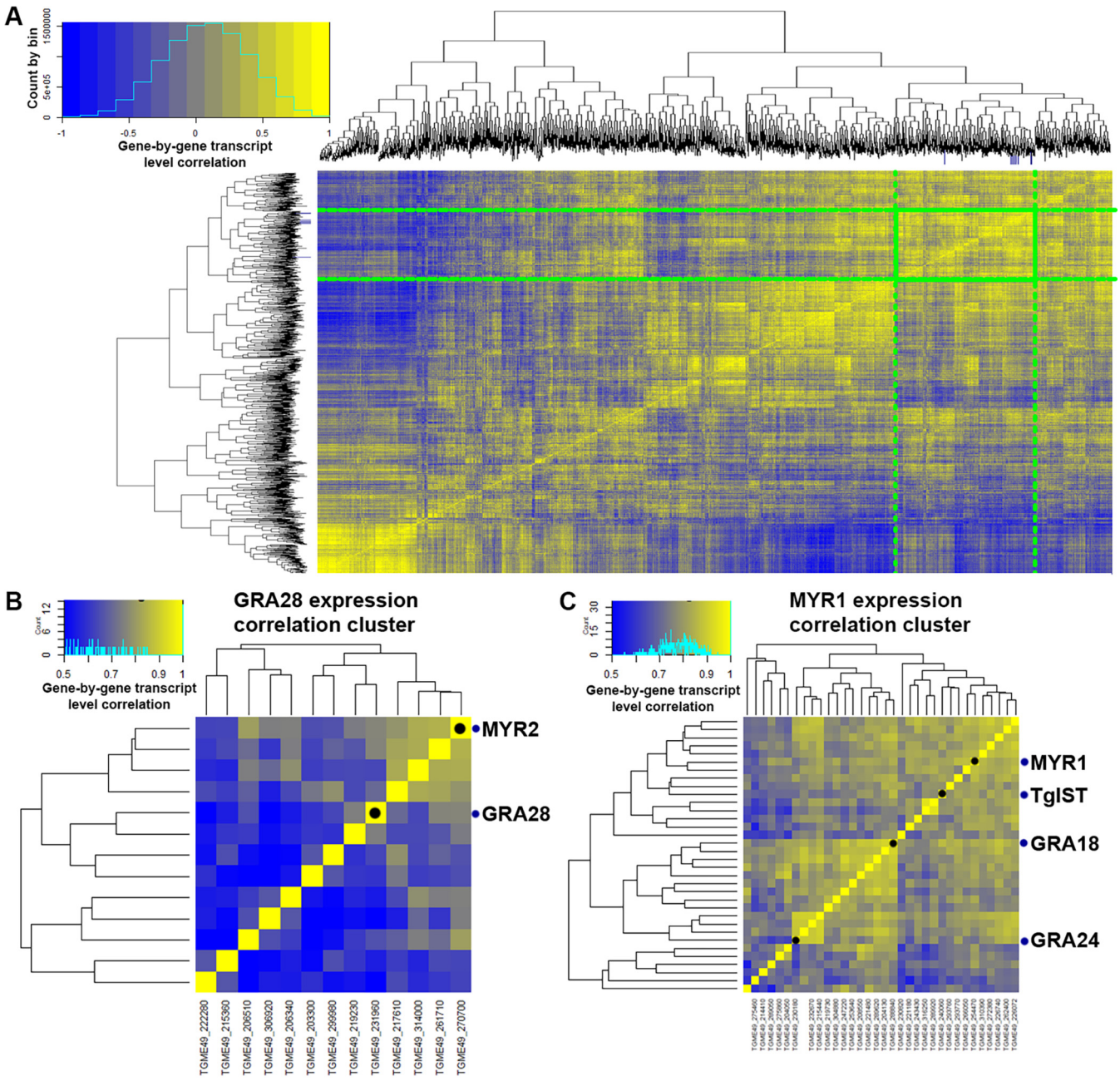

FIG 2 Transcript correlation analyses to identify putative MYR1 substrates based on 396 publicly available microarray data sets. (A) Gene-by-gene correlation data for *T. gondii* genes across 396 microarray data sets. A subset (3,217 genes with at least one sample having a normalized $\log_2$-transformed value of $\geq$10) of the total number (8,058) of *T. gondii* genes is shown for simplicity. Genes outlined in the green box indicate the cluster containing all of the bait genes as well as candidate CCL22-inducing genes, with the exception of *Toxofilin*. Dark blue tick marks on each dendrogram indicate the location of all of the bait genes. The color scale covers correlations ranging from −1 to +1. (B) Subcluster containing *MYR2* and *GRA28*. (C) Subcluster containing *MYR1*, *TgIST*, *GRA18*, and *GRA24*. It is important to note that for panels B and C, the color scale is from 0.5 to 1.0 to highlight subcluster differences.

levels (Fig. S3A), indicating that our approach could discriminate between different classes of proteins secreted from the same organelle. For example, while genes like *GRA32* (*TGME49_212300*) had transcript levels with relatively high (>0.8) correlations with bait transcript levels, other genes encoding GRA1, GRA2, and GRA11 paralogs had transcript levels that correlated much more poorly with the bait genes. This is despite the fact that most of these dense granule-encoding genes have high transcript levels compared to other gene clusters, as shown in the heat map in Fig. S3A, demonstrating that our approach yielded an additional layer of discrimination to categorize dense granule-trafficked gene products. Moreover, many of the coregulated genes are not

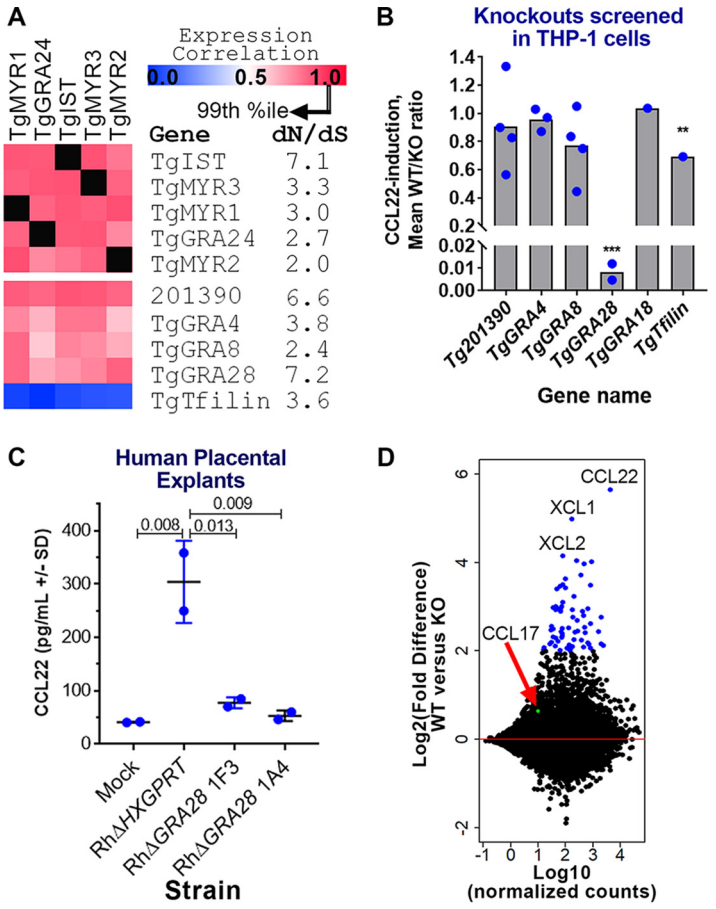

FIG 3 Identification of the *T. gondii* gene *GRA28* as an inducer of CCL22 in human cells. (A) Gene expression correlations across 396 *T. gondii* expression microarrays between Tg*MYR1* and 4 additional "bait" genes (top) and 5 candidate CCL22-inducing effectors (bottom). *dN*/*dS* ratios are also shown to illustrate the high level of positive selection acting on this class of genes. (B) Effect of deleting 5 candidate genes on CCL22 secretion in THP-1 cells, showing that Δ*GRA28* parasites induced significantly less CCL22 than wild-type controls (>100-fold reduction; ***, $P < 0.0001$). PRUΔ*Toxofilin* parasites also induced significantly lower levels of CCL22 in THP-1 cells (1.4-fold reduction; **, $P < 0.01$). Each blue dot indicates a genetically distinct knockout clone. (C) Δ*GRA28* parasite clones also induce significantly less CCL22 from primary human second trimester placental villous explants. (D) MA plot (where the $\log_2$ fold change is on the *y* axis and the log-transformed average of normalized counts is on the *x* axis) of RNA-seq analysis performed on THP-1 cells infected with WT or Δ*GRA28 T. gondii* (RH strain). CCL22 and the chemokines CXL1 and CXL2 were the most highly GRA28-dependent transcripts, while a handful ($n = 64$) of other genes had significantly higher transcript abundance in WT parasites than in Δ*GRA28* parasites ($P_{adj} < 0.001$; $\log_2FC > 2$; blue symbols). CCL17 (red arrow, green symbol), a chemokine that is typically coregulated with CCL22, did not show any evidence of being induced by GRA28.

yet annotated, but based on our analysis, one would predict that many are likely to be dense granule protein-derived secreted effectors or structural constituents of this parasite organelle.

***T. gondii GRA28* is the gene responsible for CCL22 induction in human immune and placental cells.** When we specifically examined correlations between the bait genes listed above and *MYR1*, we found that *MYR1* expression profiles were highly correlated at the transcriptional level with *MYR2/3* and *IST* (Fig. 2B and C and Fig. 3A, top), consistent with the idea that MYR1 substrates could be identified using this approach. After identifying a small list of candidate genes (Fig. 3A, bottom), we deleted each using CRISPR-CAS9, validated them using diagnostic PCR and in some cases by sequencing (Fig. S4), and screened them for CCL22 induction in THP-1 monocytes by ELISA. Among the five genes that we tested (including *GRA18*, which was recently found to induce Ccl22 in mouse macrophages [18]), we found that *GRA28* (*TGME49_231960*) was required for the induction of CCL22 secretion by infected THP-1 monocytes (Fig. 3B).

We also found that Δ*Toxofilin* parasites had significantly reduced levels of CCL22 induction (Fig. 3B), albeit to a much lesser extent than Δ*GRA28* parasites. We think it likely that this decrease is owed to the reduced invasion capacity of Δ*Toxofilin* parasites rather than a direct impact of this gene product on host CCL22 production (19, 20).

To determine if GRA28 was responsible for CCL22 production by human placental cells, we infected second trimester human villous placental explants with wild-type (WT) and Δ*GRA28* parasites and observed a marked decrease in CCL22 production by explants exposed to Δ*GRA28* parasites compared to those exposed to the WT (Fig. 3C). To gain a broader understanding of the transcriptional networks altered by *GRA28*, we compared THP-1 cells infected with RHΔ*HPT:HPT* and RHΔ*GRA28* using transcriptome sequencing (RNA-seq). A relatively small number of transcripts had significantly altered abundance when stringent statistical cutoffs were used {67 genes with an adjusted *P* value (P_{adj}) of <0.0001 and an absolute $\log_2$ fold change [abs($\log_2$FC)] of ≥ 2 are highlighted in Fig. 3D}, and these included CCL22 as well as the chemokines XCL1 and XCL2. Interestingly, transcript abundance for CCL17, a chemokine that is often coregulated with CCL22 (21, 22) and which is induced in some cells along with CCL22 by the *T. gondii* effector GRA18 (18), was not dependent on *GRA28* (Fig. 3D). The majority of transcripts that were GRA28 dependent were of higher abundance in the WT than in the Δ*GRA28* parasites when slightly relaxed statistical cutoffs were used (263 higher, 33 lower; P_{adj} of <0.05 and $\log_2$FC of ≥ 1 or ≤ 1).

We performed pathway analysis on these sets of regulated genes using Ingenuity pathway analysis (IPA) and identified host cell pathways that were either more or less induced in WT *T. gondii*-infected cells compared to RHΔ*GRA28*-infected cells (Fig. 4), including dendritic cell maturation, interleukin 6 (IL-6) and IL-8 signaling, and NF-κB signaling (Fig. 4A). When we assessed the degree of gene overlap in these gene sets, we found that 10 of the pathways contained the *JUN* and *FOS* genes (Fig. 4B), indicating a potential role for AP-1 complex-targeted transcripts in GRA28-dependent transcriptional changes. We examined correlations across these gene sets (after creating a matrix of presence/absence of each of the genes shown in Fig. 4B) and identified two nonoverlapping sets of genes. The larger cluster contains multiple immunity-related genes, while the smaller cluster contains genes involved in proteoglycan synthesis (Fig. 4C), including the *XYLT1* gene, which encodes the enzyme that adds UDP-xylose to serine residues as a first step in glycosaminoglycan synthesis. When we performed a similar analysis using the "upstream regulator" module in IPA, we identified a small set of significant (Z-score ≥ 2; $P < 0.001$) regulatory factors that were upstream of the GRA28-dependent gene set, including multiple regulators associated with the NF-κB pathway (Fig. S5A). Cluster (Fig. S5B) and downstream gene overlap (Fig. S5C) analyses further confirmed the *FOS* and *JUN* genes as contributing to the signaling pathways that were GRA28 dependent, while also confirming a putative role for NF-κB. For example, the cluster with the most similar target gene overlap contains multiple genes in the NF-κB pathway (*NFKBIA*, *NFKB1*, *RELA*) (Fig. S5C). However, when we cotransfected HEK293 cells with NF-κB luciferase reporter constructs and a construct containing the first exon of *GRA28* (see below), we saw no increase in the levels of luciferase after GRA28 transfection in contrast to a known NF-κB activating construct containing multiple caspase activation and recruitment domains (CARDs) (Fig. 4D). This suggests that NF-κB activation may not play a role in CCL22 induction. Other candidate transcriptional mediators with GRA28-dependent transcript levels are *FOS*, *JUN*, and *IRF4* (Fig. S5D). Transcript levels of *JUN* have been shown in numerous studies to increase in a variety of host cells after infection with *T. gondii* (23, 24). To test whether GRA28 played a role in altering C-JUN abundance during infection, we infected THP-1 cells with WT or Δ*GRA28 T. gondii* parasites for 24 h and using semiquantitative Western blotting to quantify C-JUN protein levels. While infection of THP-1 cells clearly increased C-JUN levels compared to that of mock-treated cells (Fig. S6), the presence or absence of GRA28 in the infecting strain had no significant impact on C-JUN protein abundance. These data suggest that while JUN transcript levels appear to be at least somewhat dependent on GRA28 in the infecting strain (Fig. S5D), this does not appear to be detectable at the protein level using Western blotting.

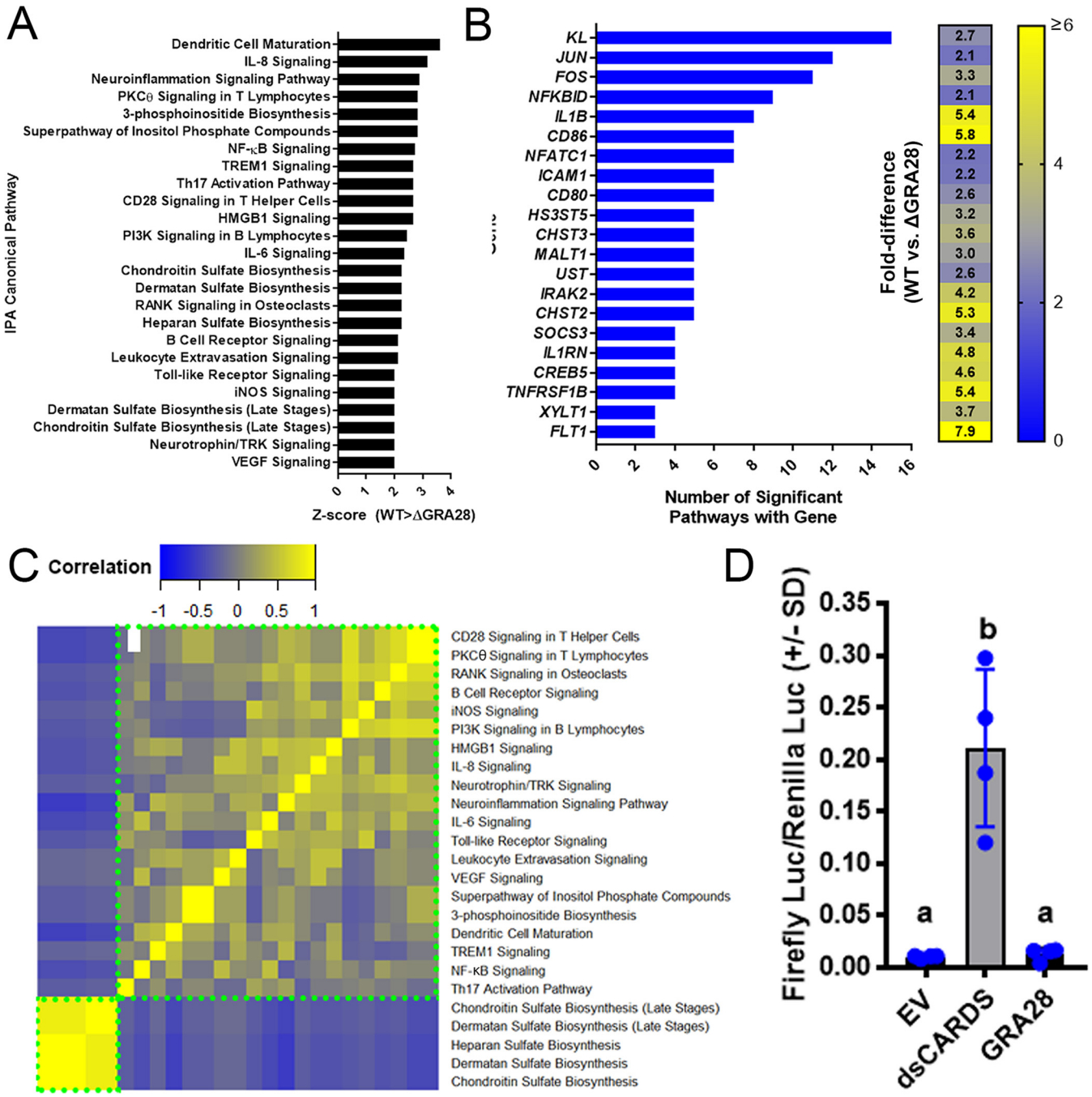

FIG 4 IPA analysis of THP-1 cells infected with WT or Δ*GRA28 T. gondii* parasites for 24 h showing canonical pathways that were differentially regulated ($-\log(P) \geq 2$; Z-score, less than or equal to −2 or greater than or equal to 2) depending on the presence or absence of the GRA28 gene. (A) Z-scores for significant canonical pathways. All were higher in WT than in Δ*GRA28 T. gondii*. (B) There was extensive overlap of component genes within each canonical pathway, particularly for the genes *KL* and those encoding components of the AP-1 transcription factor complex (*JUN* and *FOS*). A heat map of fold difference in transcript abundance for cells infected with RH WT and RHΔ*GRA28* is shown. (C) GRA28 is responsible for driving transcriptional changes in two major gene clusters identified based on the degree of gene sharing between each canonical pathway (clusters outlined in dotted green boxes). The larger cluster consists primarily of immunity-related pathways, while the smaller cluster consists of genes involved in proteoglycan synthesis. (D) Quantification of NF-κB activation in 293T cells. Cells were transfected with NF-κB firefly luciferase plasmid, a constitutive *Renilla* luciferase plasmid, as well as empty vector (EV), a construct expressing a CARD domain (dsCARDS), or the first exon of *T. gondii* GRA28. While the CARD domain construct induced firefly luciferase expression as expected, expression of *T. gondii* GRA28 had no significant impact on firefly luciferase levels (letters indicate groups that were not significantly different from one another according to one-way ANOVA and Tukey's multiple-comparison *post hoc* test.).

The first exon of *GRA28* is sufficient for induction of CCL22 during parasite infection of and ectopic expression in human cells. The *GRA28* gene has been described previously as encoding a dense granule protein that was capable of trafficking to the host cell nucleus during infection (25). However, the exact structure of the GRA28-encoding

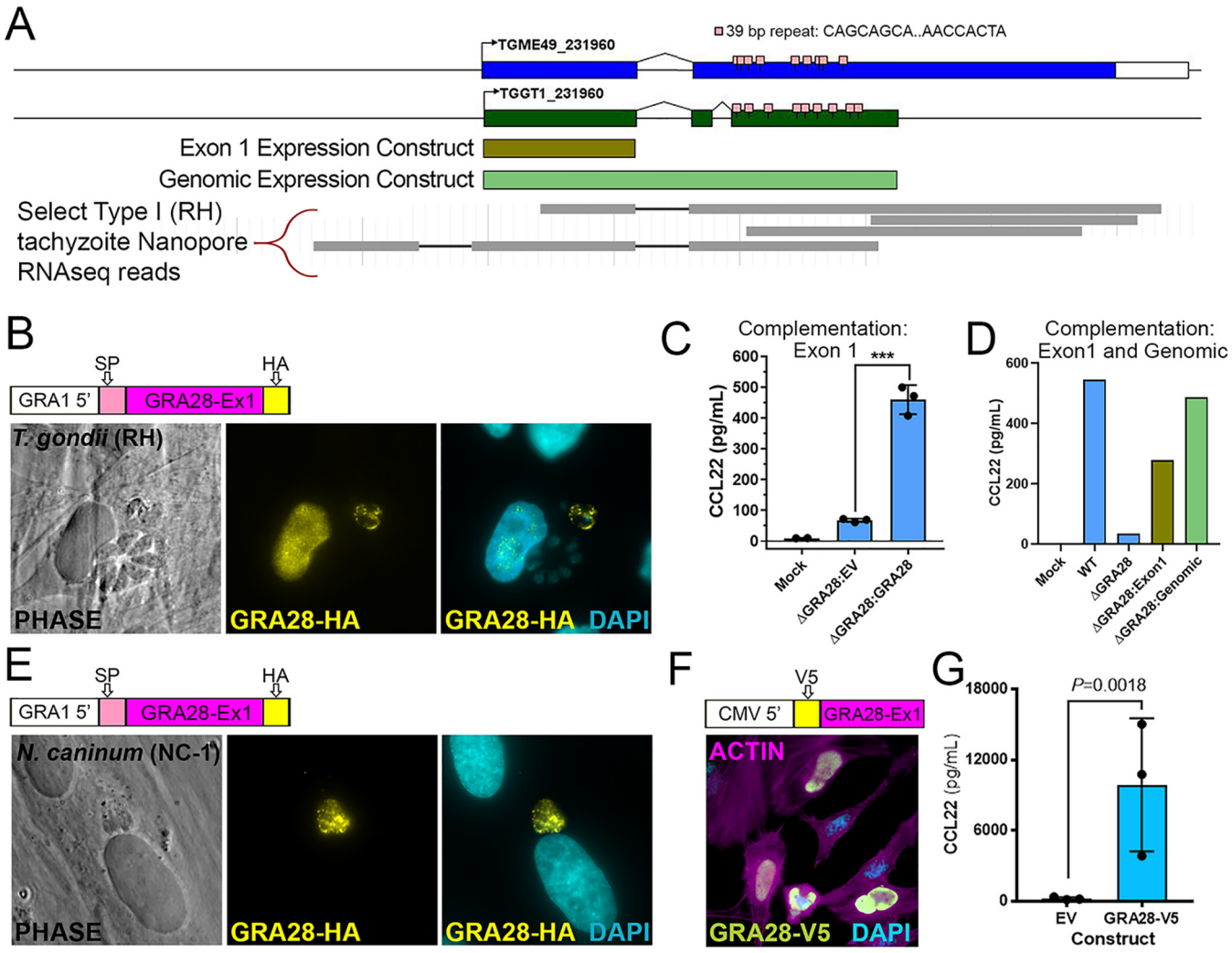

FIG 5 (A) Schematic of the *GRA28* locus along with its gene prediction in the current annotation of the *T. gondii* genome (https://toxodb.org). In addition to gene models from two *T. gondii* strains (GT1 and ME49), 39-bp repeats and regions used in expression constructs are shown in brown and light green. The map was created using GenePalette software (see Materials and Methods) (51). (B) Sequence encoding an N-terminal HA tag was inserted immediately after the predicted signal peptide cleavage site in a GRA1-promoter driven version of *T. gondii* GRA28 exon 1. When transiently transfected into *T. gondii,* HA-tagged protein could be detected in the parasites as well as the host cell nucleus. (C) Δ*GRA28 T. gondii* parasites (RH strain) were transiently transfected with empty pGRA-HA-HPT vector (EV) or the same construct described for panel B encoding an HA-tagged version of *T. gondii* GRA28 exon 1. After washing in cDMEM, parasites were used to infect freshly plated THP-1 cells for 24 h and CCL22 levels were quantified in culture supernatants using ELISA. Mock-treated cells were exposed to a sterile filtered parasite preparation. (D and E) The construct encoding HA-tagged *T. gondii* GRA28 exon 1 (same as that used for panels B and C) was used to transfect *Neospora caninum*, a near relative of *T. gondii*. HA staining revealed expression of this *T. gondii* GRA28 exon 1 in *N. caninum* parasites (visualized by HA staining), but in contrast to *T. gondii,* we did not observe trafficking of GRA28 to the host cell nucleus when expressed in this strain. Quantification of nuclear HA-derived signal is presented in Fig. S7 in the supplemental material. (F) Sequences encoding an N-terminal V5 tag were inserted downstream of a Kozak consensus sequence and upstream of GRA28 exon 1 (minus the signal peptide-encoding sequence). The construct was transfected into HeLa cells, and V5 staining was observed prominently in the nucleus of transfected cells. (G) Transfection of the construct in panel E directly into RAW 264.7 cells significantly induced CCL22 production, as detected by ELISA. A *t* test was performed on $\log_{10}$-transformed data.

gene was somewhat ambiguous based on its annotation in ToxoDB. Specifically, while TGME49_231960 is predicted as a single exon gene spanning ~7.4 kb of genomic sequence (Fig. 5A), the annotated gene is shorter in TGGT1 (Fig. 5A) and split into two gene products in *T. gondii* strains VEG, FOU, ARI, VAND, MAS, CATPRC2, and P89. The 5′ end of the gene was consistently predicted across all annotated genes, including the precise location of the first intron. When we performed *de novo* assembly of the *T. gondii* RH transcriptome, we were unable to identify any assembled transcripts that spanned the entire length of the TGME49_231960 prediction, most likely due to the fact that a 39-bp repeat in between each of these transcripts disrupted the assembly process (repeat consensus sequence, CAGCAGCAGCCACAAGGGWMTGTTGTGCATCAACCACTA) (Fig. 5A). However, it should be

noted that when we recently examined released Oxford Nanopore long-read single-molecule sequencing of *T. gondii* transcripts that are available at https://toxodb.org, there are multiple reads that span this repeat region (select Nanopore reads shown in Fig. 5A), suggesting that the gene is at least similar to that predicted for ME49 in the *Toxoplasma* genome database. Regardless, given the challenges associated with amplifying and cloning this repetitive region, we expressed a hemagglutinin (HA)-tagged version of the first exon of GRA28 in *T. gondii* and observed expression within both the parasites and the HA signal in the nucleus of infected cells (Fig. 5B). Importantly, CCL22 induction could be restored in an RHΔ*GRA28* clone after bulk transfection of the exon 1 GRA28 expression construct prior to infecting THP-1 cells (Fig. 5C), confirming the role of sequences present in the first exon of GRA28 in driving CCL22 production in human cells. Similar results were obtained when we transiently expressed a construct containing the entire genomic locus for the predicted *T. gondii* GT1 *GRA28* gene (Fig. 5A, light green bar) in RHΔ*GRA28* parasites (Fig. 5D). In contrast, when the exon 1 construct was expressed transiently in *Neospora caninum* (strain NC-1) (26), we did not observe any HA signal in the infected host cell despite expression of the protein within the parasite (Fig. 5E). When we quantified host nuclear HA signal intensity (background subtracted and then normalized to staining intensity within the parasite) (see Materials and Methods) in infected host cells, there was a clear and significant ($P = 0.0012$) difference in the amount of HA-derived signal in the host nucleus when TgGRA28 was expressed in *T. gondii* than when it was expressed in *N. caninum* (Fig. S7A). Close inspection of multiple images suggests that the trafficking of *T. gondii* GRA28 within *N. caninum* itself may be distinct from how it traffics in *T. gondii*. For example, HA staining was observed mostly within the parasite for *N. caninum* but could be found both within *T. gondii* and at the vacuole periphery (Fig. 5E; Fig. S7). While *N. caninum* clearly failed to traffic detectable amounts of GRA28 into the host cell, this could be due to (i) poor trafficking of the protein within the parasite such that it never gains proper access to vacuolar export machinery components like MYR1 and/or (ii) poor trafficking from the parasite into the host cell due to incompatibility with the *N. caninum* export machinery. Interestingly, *N. caninum* does not appear to have an intact *GRA28* gene in its genome (see the synteny map for TGME49_231960 at https://toxodB.org), although it does have a *MYR1* ortholog which has been shown to be sufficient to traffic secreted *T. gondii* proteins into the host nucleus. Finally, GRA28 exon 1 (minus the residues encoding the predicted signal peptide) could be robustly expressed in HeLa cells with a V5 tag, where it trafficked to the host cell nucleus (Fig. 5F), and also was functional when expressed ectopically in THP-1 cells, where it induced CCL22 secretion (Fig. 5F).

GRA28 induction of Ccl22 is fully conserved in mice. To determine whether parasite-driven induction of CCL22 is conserved in the murine model, we compared WT and GRA28-deficient (Δ*GRA28*) parasites for their ability to induce this chemokine *in vitro*, *ex vivo*, and *in vivo*. First, we infected mouse macrophages (RAW 264.7) *in vitro* with type 1 strain (RH) *T. gondii* parasites (WT) or RHΔ*GRA28 T. gondii* parasites at MOIs of 3. Based on Ccl22 ELISA, mouse macrophages not only release more Ccl22 protein during *T. gondii* infection, but similar to human THP-1 cells, this phenotype is also dependent on the presence of *T. gondii* secreted protein GRA28 (Fig. 6A). Next, we investigated whether primary mouse tissues, specifically mouse placental tissue, also elicit this response to *T. gondii* infection. Embryonic day 12.5 Swiss Webster mouse placentas were halved and distributed into separate treatment groups. These placental explants were then infected *ex vivo* with 2.0×10^6 type 1 strain (RH) *T. gondii* parasites (WT), RHΔ*GRA28 T. gondii* parasites, or mock treatment. As shown in Fig. 6B, primary mouse placental tissue also responds to *T. gondii* infection by releasing Ccl22 protein in a GRA28-dependent manner. RNA was also extracted from the infected placental samples, and we performed RNA-seq. As shown in Fig. 6C, the number of transcripts that varied in a GRA28-dependent manner was markedly small, suggesting that GRA28 is a highly specific inducer of *Ccl22* in mouse placental explants. Of the three genes with significantly higher transcript levels (*Ccl22*, *Il12rb2*, *Ccr7*) in wild-type 1 infections compared

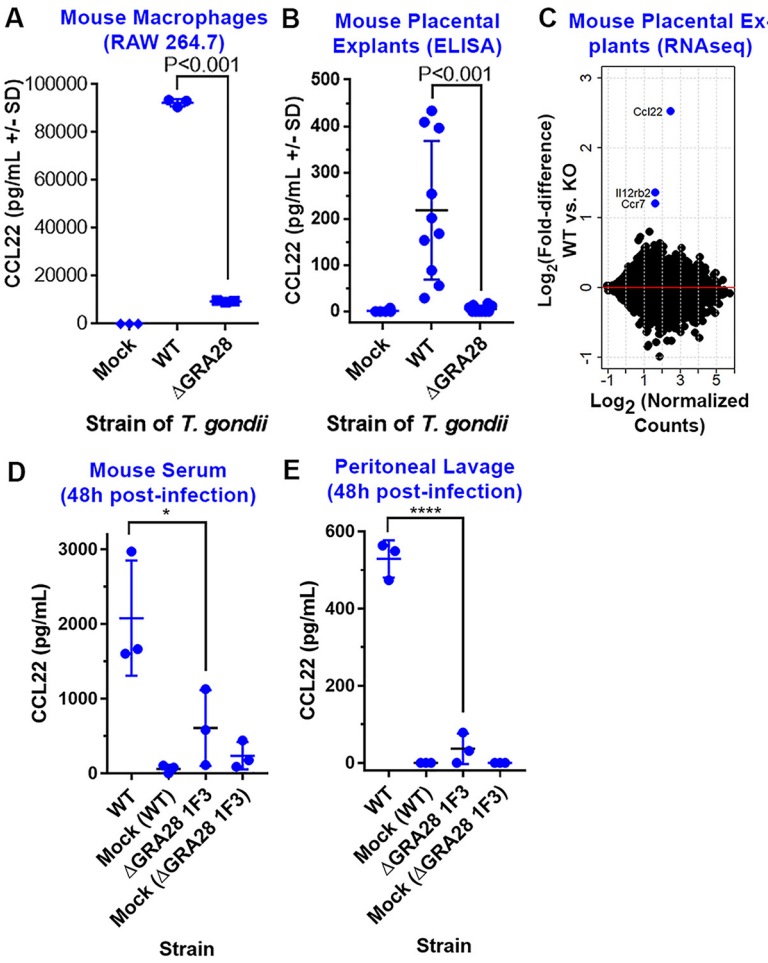

FIG 6 GRA28 induction of Ccl22 is conserved in mouse immune and placental tissues. (A and B) Δ*GRA28* parasites induce significantly less Ccl22 secretion from RAW 264.7 macrophages (A) and mouse placental explants (B) than wild-type parasites. (C) The number of host genes besides Ccl22 that are GRA28 dependent in placental explants is relatively small, suggesting that GRA28 is a highly specific inducer of Ccl22 in mouse placental tissue. (D and E) Mouse serum (D) and peritoneal lavage (E) levels of Ccl22 48 h postinfection are dependent on GRA28.

to RHΔ*GRA28* infections, *Ccl22* was the most highly induced. These data show conservation of the parasite-driven Ccl22 phenotype in primary mouse placental explants at both a protein and transcript level. Finally, we investigated mouse *in vivo* Ccl22 responses to *T. gondii* intraperitoneal infection. Female BALB/cJ mice ($n = 3$ for each treatment) were infected with WT, Δ*GRA28*, or mock *T. gondii* treatments. We focused on early, acute infection and performed Ccl22 ELISA on serum (Fig. 6D) and peritoneal lavage fluid (Fig. 6E). These suggest that *in vivo* Ccl22 protein levels are at least partially dependent on GRA28. Moreover, while there was a significant amount of systemic Ccl22 protein detected in serum of infected mice, even in the Δ*GRA28* parasite treatment, Ccl22 was almost undetectable in peritoneal lavage fluid in RHΔ*GRA28*-infected mice. Overall, these data indicate that the process driving *T. gondii* GRA28-induced Ccl22 is similar, if not the same, in both mice and humans and that this parasite effector can mediate robust changes in Ccl22 production at the site of infection and systemically.

GRA28-deficient parasites have distinct inflammatory and dissemination phenotypes in the acute and chronic phases of infection, respectively. To determine the impact of *T. gondii* GRA28 *in vivo*, we indexed differences in mouse behavior relevant to inflammatory responses and quantified differences in infection-induced weight loss and total morbidity after infection of BALB/cJ mice with either RH WT or RHΔ*GRA28 T. gondii*. We observed no significant differences in morbidity or weight loss (Fig. 7A and B). However, when we scored (Fig. S8) mice over the course of infection as to the extent of inflammation-induced behavioral

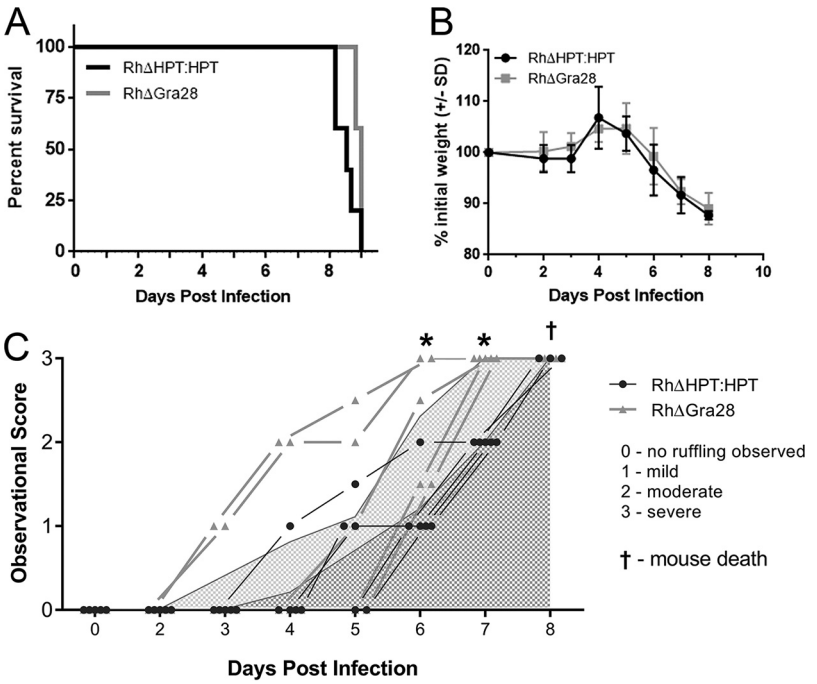

FIG 7 (A and B) Mortality (A) and weight loss (B) does not significantly differ in mice infected with WT and Δ*GRA28* type 1 strain *T. gondii* parasites. (C) Behavioral changes and fur ruffling phenotypes associated with infection are exacerbated during the acute phase of infection for mice infected with Δ*GRA28* parasites compared to that in WT parasites based on a phenotype scoring system. Specifically, mice infected with Δ*GRA28* parasites (light gray lines and triangles) exhibited infection-related symptoms at earlier time points than those infected with WT parasites (black lines and circles). Curves beneath lines are the average across all mice at that time point (with lighter gray representing Δ*GRA28* knockout parasites and darker gray representing the wild type). *, $P < 0.05$ after two-way ANOVA and followed by multiple comparisons at each time point.

changes, we observed significantly heightened fur ruffling in the RHΔ*GRA28*-infected mice on days 6 and 7 postinfection (Fig. 7C), despite the fact that mortality was unchanged.

We also generated Δ*GRA28* parasites in a type 2 *T. gondii* background that had been previously engineered to express luciferase and green fluorescent protein (GFP) (specifically ME49Δ*HPT:LUC* [27, 28]) to permit noninvasive quantification of parasite burden and dissemination over the course of infection. For the ME49 strain infections, we observed only minor and nonsignificant differences in mouse morbidity and weight loss (Fig. 8A and B). However, during the acute phase of infection, we observed slight differences in parasite burden between ME49Δ*HPT:LUC* (WT) and ME49Δ*GRA28*-infected mice, with the burden being significantly higher in ME49Δ*GRA28* than in WT mice on day 9 postinfection (Fig. 8C). This difference was not due to experimental variation in parasite input between strains, since the parasite burden was indistinguishable during the first 6 days postinfection (Fig. 8C). In contrast to these minor differences during the acute phase of infection, we observed more dramatic differences in parasite burden during the later stages of infection. Specifically, quantification of *in vivo* bioluminescence data taken dorsally on days 14 and 15 postinfection revealed that WT parasites were of much greater abundance in the brains than those infected with ME49Δ*GRA28* (Fig. 8D and E).

DISCUSSION

T. gondii-infected host cells have dramatically altered transcriptomes compared to uninfected cells, and effectors that are secreted from the parasite during invasion drive most, but not all, of these changes (29). To date, the vast majority of these parasite effectors are derived from the dense granule and rhoptry organelles. We previously identified that *T. gondii* induces the production of CCL22 in human placental trophoblasts, while human foreskin fibroblasts do not exhibit this chemokine induction during *T. gondii*

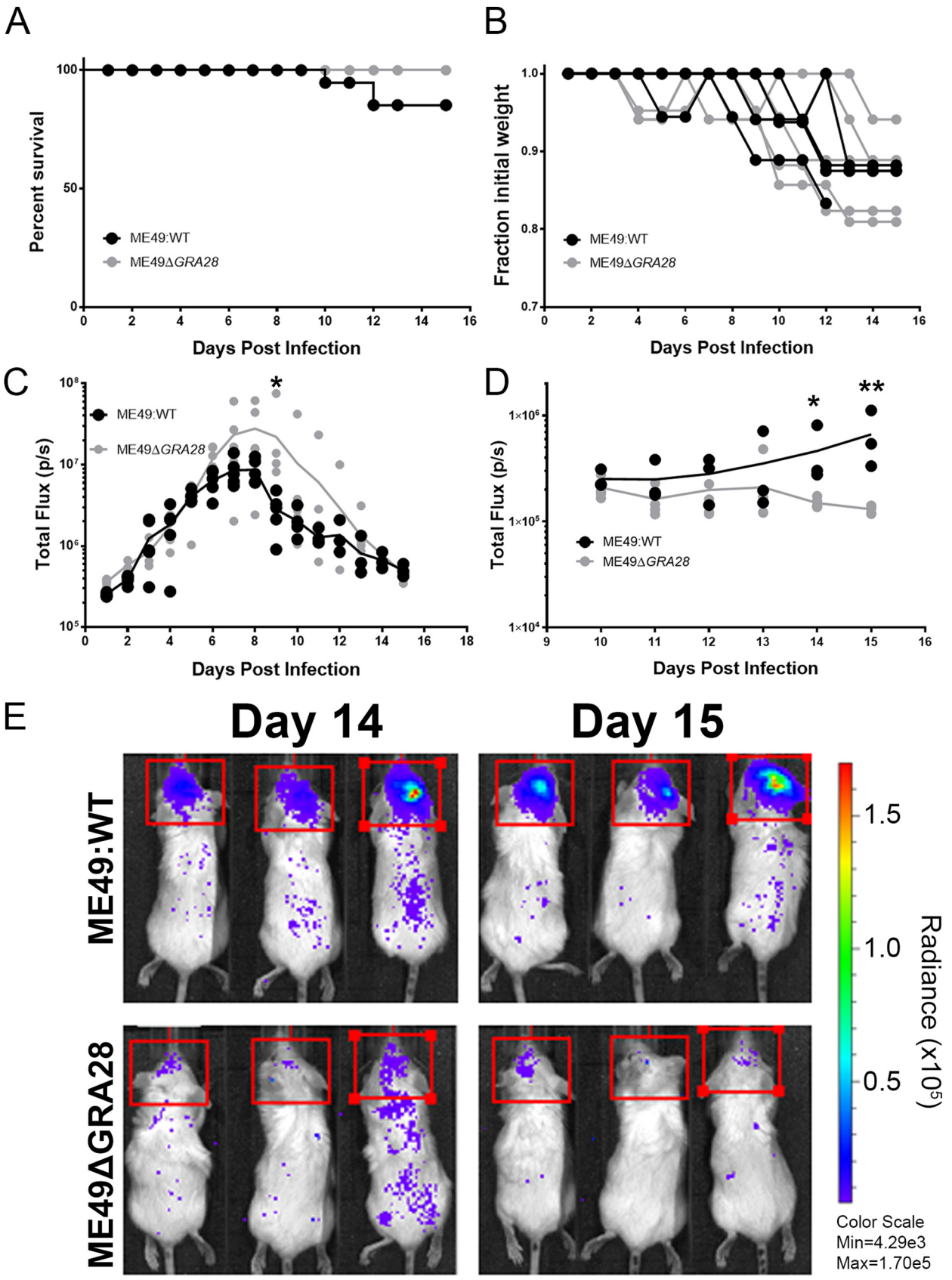

FIG 8 Impact of the *GRA28* gene on proliferation and dissemination of type 2 parasites expressing luciferase. (A and B) Neither mortality (A) nor mouse weight loss (B) was significantly different in mice infected with WT or Δ*GRA28 T. gondii* type 2 (ME49) strain parasites. (C) Throughout the

(Continued on next page)

infection (4). Additionally, our previous work has shown that this induction required parasite invasion and the effector chaperone-like *T. gondii* gene product MYR1 (4, 13). While *T. gondii* induces CCL22 during infection of a variety of cell types from both mice and humans (18, 30), including at the transcriptional level in mouse brain (31), placental cell CCL22 induction is driven by a highly specific parasite effector, GRA28. CCL22 production is considered to be an indication of M2 macrophage polarization, and macrophage polarization has been linked to strain-specific *T. gondii* effectors like ROP16 and GRA15 (32). The impact of GRA28 is distinct from these effectors because CCL22 induction occurs similarly in all three canonical strain types, and GRA28 does not alter the expression of other M2-associated genes (such as *IL-4*, *IL-10*, *IL-13*, or *ARG1*) in the cell types that we have assayed. The specificity of GRA28 for only a few target genes is novel compared to effectors like GRA15 and ROP16 (24, 33) that alter the abundance of hundreds of transcripts.

Transcriptional coregulation has been used in other systems as a means to identify members of protein complexes (34), but to our knowledge, this is the first time this approach has been successfully applied at this scale in *T. gondii*. We used 396 microarray data sets derived from multiple *T. gondii* life stages and experimental manipulations to provide enough variation to better distinguish subclusters within closely related gene families. Genes encoding dense granule proteins are among the most highly expressed in the *T. gondii* genome, making them more difficult to separate from one another, but they still clustered into two distinct groups with functional themes. The MYR1/GRA28 cluster harbored a handful of known secreted dense granule effectors, while the other contained genes encoding dense granule structural proteins or those that are secreted into the vacuole but do not traffic to the host cell. We anticipate that the former cluster can be exploited further to identify additional MYR1-trafficked, and putatively host-modulating, effectors, while the latter has highlighted new candidates important in dense granule structure or function within the parasite. The entire data set is available for download as a text file at Figshare (https://doi.org/10.6084/m9.figshare.16451832) so that these data can be mined to identify candidates for membership in other critical *T. gondii*-specific protein complexes.

GRA28 was previously shown to encode a dense granule protein secreted from the parasite into the host cell, where it trafficked to the host cell nucleus (25), but its impact on the host cell was unknown. Its natural presence in the host nucleus during infection has also been further confirmed using proteomics, where it was found to be one of the more abundant *T. gondii* proteins in the nucleus of the infected host cell (35). The fact that it affects the abundance of only a small number of chemokine-encoding genes at the transcriptional level suggests that it modulates transcriptional activity via direct interactions with transcription factors and/or upstream regulatory sequences. Other *T. gondii* effectors traffic to the host nucleus, but this is not always critical for function. For example, ROP16 localization to the host cell nucleus is dispensable for its primary function of phosphorylating STAT6, which occurs in the cytoplasm of the host cell (36). Other *T. gondii* effectors like IST (15, 37) and GRA24 (16) function within the host cell nucleus, but many of these mediate changes in hundreds of transcripts via their cooperation with existing transcriptional suppressors (IST [15, 37]) or activators (GRA24 [16]). It remains to be seen if the function of GRA28 can occur independently of nuclear trafficking or if this ultimate localization is required for chemokine induction, but its specificity for downstream genes raises the interesting hypothesis that it may function directly, possibly as a heterologous transcription factor.

The signaling pathway governing GRA28 function is unknown, but some clues can be found in our pathway analyses, which suggest a role for GRA28 in mediating changes in key immunity-related host cell signaling pathways. The transcription factor genes *JUN*, *FOS*, and

FIG 8 Legend (Continued)
acute phase of infection, parasite-derived bioluminescence of WT and Δ*GRA28* parasites in the peritoneal cavity was measured by imaging the animals ventrally. The burdens were similar ($P > 0.05$) between parasite strains at all time points except for day 9 postinfection, when the signal was significantly higher in Δ*GRA28*-infected mice than in WT mice ($P = 0.014$). (D and E) Starting on day 10 postinfection, we imaged mice both ventrally and dorsally to visualize dissemination to and proliferation in the mouse brain. In contrast to findings for the acute phase, we observed a consistently lower level of parasite-derived bioluminescence in the brains of mice infected with Δ*GRA28* parasites than with WT parasites on days 14 and 15 postinfection ($P = 0.016$ and 0.0002, respectively). All statistical tests were performed on $\log_2$-transformed bioluminescent data.

components of the NF-κB complex were consistently linked to the GRA28-dependent host transcripts. Lipopolysaccharide (LPS) is a well-known activator of both NF-κB and C-Jun activity in THP-1 cells (38, 39), and this can occur via Toll-like receptor activation (40). However, *T. gondii* induction of CCL22 was not fully dependent upon host MYD88, since MYD88$^{(-/-)}$ THP-1 cells still produced significant amounts of CCL22 in response to *T. gondii* infection (see Fig. S1C in the supplemental material). The difference in CCL22 production by the MYD88$^{(-/-)}$ cells in comparison to the WT cells should also be considered in light of the fact that the cell lines have different origins (and therefore distinct passage histories, which could have the more subtle effects shown on CCL22 production after infection). A distinct cluster of GRA28-dependent host genes was identified that encoded gene products involved in proteoglycan synthesis, including the rate-limiting enzyme XYLT1. *T. gondii* attachment to host cells is mediated by interactions between parasite adhesins and host cell surface sulfated proteoglycans (PG) like heparan sulfate (41, 42), and *T. gondii* adheres poorly to cells with genetically or enzymatically depleted levels of surface sulfated proteoglycans (41, 42). Therefore, direct and/or indirect modulation of XYLT1 transcript levels by GRA28 may serve to make infected cells susceptible to adhesion, and ultimately invasion, by *T. gondii* or any other pathogens that depend on surface proteoglycans.

GRA28 had no impact on transcript levels of the gene encoding CCL17, which is commonly coregulated with *CCL22*. Mouse macrophages infected with *T. gondii* produce Ccl17 and Ccl22, and this is due, at least in part, to another *T. gondii* effector, GRA18 (18). Using the same *GRA18* knockout lines (kindly provided by the Bougdour lab), we found that GRA18 had no impact on CCL22 production at the transcriptional (not shown) or protein (Fig. 4) level in human THP-1 cells, suggesting that GRA18 and GRA28 have distinct targets. This is also consistent with the observation that Ccl22 induction in RAW macrophages is only partially dependent on GRA18 and β-catenin signaling, in contrast to Ccl17 and Ccl24. Finally, in our work, we used lower MOIs (2 to 3 here compared to 5 to 6 in reference 18). Regardless, GRA28 appears to be the more potent modulator of Ccl22 production compared to GRA18, while Ccl17 appears to be much more dependent on GRA18. It is exciting to speculate that *T. gondii GRA28* has evolved to uniquely target CCL22 as a means to gain access to the fetal compartment, since this chemokine is potently induced in placental cells and this chemokine plays a role in immune tolerance during pregnancy (7). However, as shown clearly in this study, GRA28 also alters monocyte/macrophage CCL22 production, making it equally plausible that this intricate molecular relationship developed first as a more generalized immune evasion (via suppression) strategy.

The role of specific chemokines like CCL22 during *T. gondii* infection is poorly understood, but the discovery of *GRA28* allows this to be addressed more directly using *T. gondii* Δ*GRA28* parasites from different genetic backgrounds. Hypervirulent *T. gondii* RH strain Δ*GRA28* parasites caused inflammation-related behavioral changes earlier during infection in mice in comparison to mice infected with WT parasites, suggesting that GRA28 functions to suppress inflammatory responses (likely due to induction of CCL22, although we did not test this directly). This could arise via GRA28-mediated recruitment and/or activation of regulatory T cells to the site of infection. These behavioral changes occurred without an effect on the acute virulence phenotype, as all mice succumbed to the infection with similar kinetics, which is consistent with an impact of GRA28 on suppressing inflammatory responses without altering the ability of the mouse to control parasite replication. However, after infections using the type 1 parasite genotype, we observed a significant reduction in Δ*GRA28* parasite burden in the brain compared to that of wild-type parasites. This effect was unexpected, given the fact that the parasite burdens were statistically the same during the acute phase of infection, but points to a potential important role for GRA28 in altering the host innate immune response in a manner that increases host susceptibility to dissemination of *T. gondii* across critical barriers like that guarding the central nervous system (CNS). *T. gondii* can infect blood-brain barrier epithelial cells as a means to cross into the host CNS (43), so GRA28 may promote parasite survival at this critical interface by recruitment of regulatory T cells or other cell types that might downregulate inflammatory responses.

Summary. Taken together, our data point to a specific role of *T. gondii* GRA28 in modulating chemokine production in the infected cell. Importantly, this effect occurs only in certain cell types, including cells from both human and mouse placenta. A relatively small number of host chemokines are affected by parasites expressing this gene, and it plays a role in both modulation of the inflammatory response (as evidenced by mouse behavior and appearance during infection) and ultimately parasite dissemination to "privileged" sites like the CNS.

MATERIALS AND METHODS

Cell culture. All cell and tissue cultures were incubated at 37°C and 5% CO_2. All media were supplemented with 10% fetal bovine serum (FBS; Atlas Biologicals), 2 mM L-glutamine, and 50 mg/ml penicillin-streptomycin. Human foreskin fibroblast (HFF) cells were grown in Dulbecco's modified Eagle medium (DMEM; Gibco), Raw264.7 cells were grown in DMEM (Gibco) with 10 mM HEPES, and THP-1 cells were grown in RPMI 1640 medium (Corning). THP-1 cells were assayed for viability using trypan blue staining (0.4%) (Gibco), counted, and spun at 120 × *g* for 10 min at 24°C, and the medium was replaced with supplemented DMEM prior to infection. All THP-1 cell numbers listed are based on trypan blue-negative cells. Media containing serum, glutamine, and antibiotics are called "complete" and have a prefix of "c" in the text (e.g., cDMEM).

Human placental explants. Human placental tissue from less than 24 weeks of gestation was obtained, cultured, and infected with *T. gondii* as described previously (44).

Mouse placental explants. Mouse placental tissues were obtained by dissection of embryonic day 12.5 (E12.5) or E18.5 Swiss Webster mice. Upon removal of the fetuses from the mother, the placentas were dissected away from other tissues and placed into prewarmed 37°C phosphate-buffered saline (PBS). The placentas were washed three times in fresh prewarmed PBS. Each placenta was then cut in half with sterilized surgical scissors, and each half was placed into a well on a plate with prewarmed 37°C DMEM with 10 mM HEPES, 10% FBS, 2 mM L-glutamine, and 50 mg/ml penicillin-streptomycin. Each placenta had one half-piece of tissue represented in each treatment group. For *T. gondii* infections, isolated tissue was infected immediately with 5.0×10^5 to 2.0×10^6 parasites for ~24 h.

Parasites. Type 1 (RH, GT1), type 2 (Me49, PRU), and type 3 (Veg, CEP) *Toxoplasma gondii* tachyzoites and sporozoites, *Neospora caninum* (NC-1) tachyzoites, and *Hammondia hammondi* (HhCatAmer and HhCatEth1 [45, 46]) sporozoites were used in this study. Sporozoites were excysted from sporulated oocysts as described previously (47) and either used immediately or grown for 24 h in HFFs prior to being used in controlled infections. Tachyzoites were maintained by continual passage in HFF cultures incubated at 37°C and 5% CO_2 in DMEM supplemented with 10% FBS (Atlas Biologicals), 2 mM L-glutamine, and 50 mg/ml penicillin-streptomycin. The RH*YFP* strain was a gift from David Roos (University of Pennsylvania), the RHΔ*MYR1* and RHΔ*MYR1:MYR1*$_c$ parasites (13) were a gift from John Boothroyd (Stanford University), the PRUΔGRA18 and complemented knockout parasites were shared by Alexandre Bougdour (18), and the PRUΔ*Toxofilin* KO parasites (19) were a gift from Melissa Lodoen (UC Irvine). For infections, infected monolayers were washed with fresh cDMEM and then scraped and syringe lysed to release tachyzoites. These tachyzoites were then passed through a 5-μm syringe filter and counted. Parasites were then centrifuged at 800 × *g* for 10 min at 24°C and resuspended and diluted in cDMEM before being used in infections. Mock treatments were produced by filtering the same parasites through a 0.22-μm syringe filter and exposing host cells to the same volume of the filtrate as was used for parasite infections. Freeze treatments were produced by subjecting the parasites to −80°C for 15 min, fixation treatments were produced by exposure to 4% paraformaldehyde for 10 min followed by washing in PBS, and sonication treatments were produced by sonication at 0°C using five 30-s bursts at 50 A with 30-s cooling intervals between bursts, followed by microcentrifugation at 800 × *g* for 10 min to generate soluble (S) and pellet (P) fractions.

Invasion inhibitor assays. For cytochalasin D (Cyt-D) treatment, parasites were pretreated with 10 μg/ml of Cyt-D in cDMEM for 1 h and then used to infect cells in the presence of 10 μg/ml of Cyt-D in cDMEM for the duration of infection. Vehicle of Cyt-D is dimethyl sulfoxide (DMSO) (40 μl per ml of cDMEM). For 4-bromophenacyl bromide (4-BPB) treatment, parasites were pretreated with either 0.5 or 1 μM 4-BPB for 15 min. 4-BPB was dissolved directly in cDMEM. Parasites were then washed twice with normal cDMEM with 10-min 800 × *g* spin steps between each wash and then used to infect cells in the presence of normal cDMEM.

Plaque assays. Parasites were serially diluted in medium and used to infect monolayers so that each tissue culture flask of HFFs received 100 parasites. These flasks were then incubated at 37°C in 5% CO_2 undisturbed for 5 to 7 days. At the end of the incubation period, each flask was counted for number of plaques present and parasite viability was calculated. Crystal violet staining was used to count plaques as follows: the monolayer was washed with PBS and fixed for 5 min with ethanol. Then, crystal violet solution (12.5 g crystal violet in 125 ml ethanol mixed with 500 ml 1% ammonium oxalate in water) was introduced to the monolayer and allowed to stain for 5 min. The monolayer was then washed extensively with PBS and allowed to air dry prior to the counting of plaques.

Candidate gene identification using transcript level correlation analysis. To identify candidate effectors for inducing CCL22, we exploited the fact that the CCL22 induction response in THP-1 and placental cells required the presence of the *T. gondii* effector translocation protein MYR1 (13, 14). We hypothesized that MYR1-dependent effectors would have similar transcript abundance profiles across diverse expression data sets. We downloaded 396 publicly available *T. gondii* microarray expression data sets from the Gene Expression Omnibus platform hosted by the NCBI (48). We loaded and processed each CEL file using the "affy" module implemented in R (49). Data were processed and normalized using the following commands: bgcorrect.method = "rma," normalize.method = "quantiles,"

pmcorrect.method = "pmonly," summary.method = "medianpolish". RMA-normalized data were exported, reimported into R, and then transposed. An all-versus-all Pearson correlation matrix was generated using the "cor" function from the R:Stats base module. Probe names on the Affymetrix array (in the format of XX.mXXXXXX) were converted to current TGME49 gene models using data downloaded from ToxoDB and the Vlookup function in Microsoft Excel. In some cases, the microarray annotations could not be matched to current TGME49 gene model names and are shown as blanks in plots. This correlation matrix, the normalized array data used to generate it, and a key to convert Affymetrix probe names to current gene model names are all available on Figshare (https://doi.org/10.6084/m9.figshare.16451832). To analyze this correlation matrix, we used hierarchical clustering tools implemented in R, including heatmap.2 (from the gplots package) and the dendextend package. To identify candidate genes using this matrix, we calculated the mean correlations between 5 bait genes and all other queried genes from the microarray. The bait genes were known to encode either components of the MYR complex themselves or known TgMYR substrates (TgMYR1 [13], TgMYR2 and TgMYR3 [14], TgGRA24 [16], and TgIST [15]). Most of the candidate CCL22-inducing genes were identified based on having (i) an average correlation with the 5 above-listed "bait" genes of $\geq$0.7, (ii) a *dN*/*dS* ratio of $\geq$2, and (iii) the presence of a predicted signal peptide or at least one transmembrane domain (which we reasoned could be a cryptic signal peptide if the wrong start codon was chosen for the current gene annotation).

***De novo* transcript assembly.** To identify and assemble transcripts coding for GRA28, we used the *de novo* transcript assembler Trinity (50) (version 2.6.6; default settings) using triplicate RNA-seq data sets from WT *T. gondii* RH parasites infecting THP-1 cells (see below). Assembled transcripts with similarity to the predicted *GRA28* gene (TGME49_231960) were identified using BLASTN and BLASTX. Primary plots were generated using GenePalette software (51) and then modified.

CRISPR-mediated gene disruption and validation of knockouts. The pSAG1::CAS9-U6::sgUPRT plasmid provided by David Sibley (Addgene plasmid no. 54467 [52]) was modified using the Q5 site-directed mutagenesis kit (NEB) so that the guide RNA (gRNA) sequence was replaced with two restriction enzyme sites (sequence, GTTTAAACGGCCGGCC) for PseI (NEB R0560S) and FseI (NEB R0588S). This modified plasmid was then used as the template for all future Q5 reactions. Two unique gRNA sequences were created for each candidate gene by utilizing the genomic sequences for *T. gondii* GT1 (https://toxodb.org) and E-CRISP (www.e-crisp.org) using the ToxoDB-7.1.31 reference genome. A forward primer for each gRNA was created for use with the modified pSAG plasmid, with the unique gRNA sequence followed by a section of the plasmid scaffolding (GTTTTAGAGCTAGAAATAGCAAG). The reverse primer used with this plasmid is AACTTGACATCCCCATTTAC. The gRNA sequences for the genes mentioned in this study and the primers used to validate the knockouts are listed in Table S1 in the supplemental material.

A plasmid was created for each gene of interest (GOI) using the modified pSAG plasmid template and the Q5 site-directed mutagenesis kit (NEB) by following the manufacturer's protocol with a few adaptations. The KLD enzyme step was extended to 60 min of incubation at room temperature, and following the KLD enzyme step, the product was heated to 65°C for 20 min and then double digested with PseI and FseI in CutSmart buffer (NEB) for 60 min at 37°C to remove any remaining plasmid that was not eliminated by the DpnI in the KLD step. This digested product was then heated to 65°C for 20 min to deactivate the enzymes prior to transformation, plasmid isolation, and sequencing to validate insertion of the correct gRNA sequence (pSAG:GOI:gRNA). Parasites were transfected with either a single gRNA plasmid or equal amounts of plasmids encoding two gRNAs targeting the same gene. For validation of knockouts after cloning, a clone was considered a knockout if PCR across a targeted cut site failed or if a PCR across the entire gene (just upstream and downstream of the start and stop codons, respectively) failed. In some cases where all PCRs worked (indicating that the plasmid failed to insert at the gRNA target site), the amplified band was sequenced and a clone was considered a knockout if insertions/deletions were identified near the gRNA binding that resulted in frameshifts and premature stop codons. Validation data for all knockout strains used except the *T. gondii* Δ*Toxofilin* parasites (which were provided by Melissa Lodoen, University of California-Irvine) are shown in Fig. S4.

Parasite transfections. In general, transfections were performed using standard approaches. Briefly, parasite suspensions were obtained by needle passage (25- and 27-gauge needles) and then pelleted for 10 min at 800 $\times$ *g*. Parasites ($\sim 2 \times 10^7$ per transfection) were resuspended in Cytomix (120 mM KCl, 0.15 mM $CaCl_2$, 10 mM KPO_4, 25 mM HEPES, 2 mM EDTA, 5 mM $MgCl_2$, pH 7.6) containing glutathione (GSH) and ATP and electroporated at 1.6 kV with a capacitance setting of 25 μF using a BTX ECM600 electroporator. Transfected parasites were then used to infect coverslips and/or flasks of confluent HFFs and placed under appropriate selection. For candidate gene knockouts, $\sim 2 \times 10^7$ *T. gondii* RHΔ*HPT* parasites were transfected with $\sim$30 to 50 μg of the relevant pSAG:GOI:gRNA plasmid(s) (described above) along with 2 to 5 μg of an empty pGRA-HA-HPT (53) plasmid. Parasites were placed under selection the next day and cloned by limiting dilution after 2 to 3 passages. Individual clones were screened for gene deletion by PCR and sequencing to permit identification of both target gene disruptions (via insertion of the pGRA-HA-HPT plasmid at the CAS9 cut site) or mutation via DNA repair events at the CAS9 cut site. For HA-tagging experiments, type 1 (RH) *GRA28* exon 1 (residues 1 to 498) was C-terminally HA tagged by cloning into the *T. gondii* expression plasmid pGRA-HA-HPT (53). This plasmid drives protein expression using the highly active *GRA1* promoter. TgRHΔ*HPT* or *N. caninum* Liverpool (NcLIVΔ*HPT*) (54) parasites were transfected with $\sim$40 to 60 μg of *GRA28* exon 1 plasmid, and cells were grown overnight in normal medium. For analysis of transiently transfected parasites, cells were only grown for 18 h post-transfection, while for stable transfection, parasites were grown for 2 to 3 passages in medium containing 50 μg/ml of mycophenolic acid and xanthine. Cells were fixed with 4% paraformaldehyde (PFA) and permeabilized in 0.1% Triton–PBS. Samples were probed with anti-HA rat monoclonal antibody (3F10 clone; Roche) diluted to 0.1 mg/ml in 0.1% Triton–PBS buffer and washed four times in PBS. Samples

were then incubated in 488 goat anti-rat antibody (Life Technologies, Alexa Fluor H+L), followed by PBS washes. All samples were mounted in Vectashield with DAPI (4′,6-diamidino-2-phenylindole) (Vector Laboratories). For genetic complementation, TgRHΔ*GRA28* parasites were transfected with the exon 1 construct described above or a construct amplified from genomic DNA encompassing the start and stop codons of the GT1 version of GRA28 (TGGT1_231960). Expression plasmids (~30 μg) were cotransfected along ~5 μg of pLIC_3×HA_DHFR* plasmid (kindly provided by Vern Carruthers) (55), and populations were placed under 1 μM pyrimethamine selection for 2 to 3 weeks and then used to infect THP-1 cells for 24 h as described above, followed by assays to quantify CCL22 in culture supernatants by ELISA.

Fluorescence image analysis. To compare signal intensities in the nucleus of host cells infected with either *T. gondii* or *N. caninum* parasites transiently transfected with the HA-tagged GRA28 exon 1 construct, we scanned stained coverslips for GRA28-HA-positive vacuoles and then used Fiji (an implementation of ImageJ) to calculate (i) the average HA signal intensity in the nucleus of the infected host cell (*AvgIntInf*), (ii) the average HA signal intensity in the nucleus of a neighboring, uninfected host cell (*AvgIntUninf*), and (iii) the average signal intensity of the parasite-containing vacuole (*AvgIntVacuole*). We then used the following calculation to determine the normalized, background-subtracted nuclear signaling intensity:

$$\frac{(AvgIntInf - AvgIntUninf)}{AvgIntVacuole}$$

Example images of this process are shown in Fig. 5 and in Fig. S7 in the supplemental material. Data were $\log_{10}$ transformed prior to performing a Student's *t* test.

RNA-seq. RNA was isolated from cultures using the RNeasy minikit (Qiagen) and its associated RNase-free DNase digestion set (Qiagen), in accordance with the manufacturer's protocol for mammalian cells. An Agilent bioanalyzer was used to check the quality of the RNA samples. Tru-Seq stranded mRNA libraries were generated from 5 to 17 ng/μl of mRNA for THP-1 cells, and from 50 to 120 ng/μl of mRNA for murine peritoneal exudate cells (PECs) and placental explants, and sequenced with an Illumina NextSeq 500 sequencer. mRNA-Seq FASTQ reads were mapped to the human reference genome (*Homo sapiens* v81; hg38) using default options on CLC Genomics Workbench 11 (Qiagen). Total gene reads (with at least 1 read count) were exported from CLC Genomics Workbench and used for DESeq2 (56) to perform differential expression analysis using methods outlined previously (for an example, see reference 4). Data were evaluated using principal-component analysis (embedded in the DESeq2 package), and genes were deemed to be significantly expressed if the $\log_2$ fold change was greater than or equal to 1 or less than or equal to −1 and with an adjusted *P* value (P_{adj}) value of <0.01. Gene set enrichment analysis (GSEA) (57) and Ingenuity pathway analysis (Qiagen) (58) software were used to compare gene sets that were differentially regulated after infection with WT and Δ*GRA28* parasites.

CCL22 and Ccl22 ELISA. CCL22/Ccl22 ELISAs were performed on culture supernatants (undiluted or diluted when necessary) using Immulon 4HBX flat-bottom microtiter plates with the human CCL22/MDC DuoSet ELISA (R&D Systems DY336) or the mouse Ccl22/Mdc DuoSet ELISA (R&D Systems DY439) per the manufacturer's instructions.

Mouse experiments with WT and Δ*GRA28* parasites. To determine the impact of *T. gondii* candidate effectors on mouse morbidity and cytokine production, BALB/cJ mice from Jackson Laboratories (4 to 6 weeks old, female) were injected intraperitoneally with 200 μl of PBS containing 1.0×10^6 *T. gondii* tachyzoites or with 200 μl of 0.22-μm-pore-size-filtered parasite solution as a mock treatment. Mice were sacrificed at 48 h postinfection (hpi), and PECs were collected by injecting 3 ml sterile PBS into the abdominal cavity, rocking the mouse to mix the PBS, and siphoning the PBS solution into a sterile conical tube. The solution was then centrifuged at 1,000 × *g* for 10 min at 24°C, the supernatant was collected, and RNA was extracted from the pellet for reverse transcription-quantitative PCR (RT-qPCR) and RNA-seq. Blood was collected in Sarstedt Microvette CB 300 Z tubes by cardiac puncture and centrifuged at 10,000 × *g* for 5 min to separate the serum. Mice were infected with RHΔ*HPT* (wild type), RHΔ*MYR1*, or RHΔ*GRA28* parasites depending on the experiment.

To determine the impact of *GRA28* deletion on *T. gondii* proliferation and dissemination, female BALB/cJ mice (4 weeks old) from Jackson Laboratories were injected intraperitoneally with 200 μl PBS containing 100 *T. gondii* tachyzoites. In one experiment, five mice received an injection of RHΔ*GRA28* parasites, while the other five received an injection of the transfection control parasite that was transfected with empty vector (RHΔ*HPT*:*HPT*). For behavioral indices of inflammatory responses, photographs of the mice were taken dorsally and laterally every 4 to 6 h for the entire duration of the infection. Mice were visually scored 0 to 3 based on the presence of fur ruffling, the location of ruffling, and the presence of skin redness/irritation (Fig. S8), as follows: 0, no fur ruffling or red/irritated skin present; 1, mild ruffling present, located predominantly on the head and back of the neck; no red/irritated skin visible; 2, moderate ruffling present—fur forms larger clumps and extends to the rest of the body; skin may be visible through the clumps but is not red or irritated; 3, severe ruffling characterized by fur ruffling present across the entire body with visibly red/irritated skin in between fur clumps.

In a second experiment, mice were infected with 1,000 tachyzoites of *T. gondii* strain ME49:*LUC*Δ*GRA28* or a passage-matched wild-type strain (27, 28). Mice were imaged daily after injection of D-luciferin as described previously (28, 59) using an IVIS Lumina II *in vivo* bioluminescence imaging system (with ventral imaging occurring on all days postinfection and ventral and dorsal imaging occurring starting on day 10 postinfection). Animals were anesthetized using 2% isoflurane during the 4- to 8-min imaging period (ventrally and dorsally where applicable). When necessary, blood was collected via submandibular lancet puncture, collected into Sarstedt Microvette CB 300 Z tubes, and spun at 10,000 × *g* for 5 min to separate the serum. Mice were monitored extensively over the course of infection for symptoms of morbidity and humanely euthanized. All animal

procedures were approved by the Division of Laboratory Animal Resources and IACUC, and our animal facilities are routinely inspected by the USDA and the local IACUC.

Statistics. All statistics were performed in GraphPad Prism for Windows (versions 7 or 9; GraphPad Software, La Jolla, CA). For most two-treatment assays, we used an unpaired, two-tailed Student's *t* test, and for multitreatment/condition experiments, we used one- or two-way analysis of variance (ANOVA) followed by multiple-comparison *post hoc* tests. Individual comparisons are listed for each assay in the text and figure legend, and only preplanned comparisons were performed to minimize type 1 errors. *In vivo* bioluminescence data (total flux; photons/s) and nuclear staining intensity data (comparing nuclear trafficking of *T. gondii* GRA28 when expressed in *T. gondii* or *N. caninum*) were $\log_{10}$ transformed prior to statistical analysis.

SUPPLEMENTAL MATERIAL

Supplemental material is available online only.

FIG S1, JPG file, 0.5 MB.

FIG S2, JPG file, 1.7 MB.

FIG S3, JPG file, 1.1 MB.

FIG S4, PDF file, 0.5 MB.

FIG S5, JPG file, 1.3 MB.

FIG S6, JPG file, 1.2 MB.

FIG S7, JPG file, 0.5 MB.

FIG S8, TIF file, 1.6 MB.

TABLE S1, DOCX file, 0.01 MB.

ACKNOWLEDGMENTS

We thank Alexandre Bougdour (INSERM, Grenoble, France) for providing *GRA18* knockout and complemented strains, John Boothroyd and Michael Panas (Stanford University) for helpful discussions and providing *MYR1* knockout and complemented strains, and Peter Bradley (University of California–Los Angeles) for helpful discussions and sharing reagents related to GRA28 that facilitated this work.

REFERENCES

1. Fallahi S, Rostami A, Nourollahpour Shiadeh M, Behniafar H, Paktinat S. 2018. An updated literature review on maternal-fetal and reproductive disorders of *Toxoplasma gondii* infection. J Gynecol Obstet Hum Reprod 47:133–140. https://doi.org/10.1016/j.jogoh.2017.12.003.
2. Stagno S, Reynolds DW, Amos CS, Dahle AJ, McCollister FP, Mohindra I, Ermocilla R, Alford CA. 1977. Auditory and visual defects resulting from symptomatic and subclinical congenital cytomegaloviral and *Toxoplasma* infections. Pediatrics 59:669–678.
3. Fahnehjelm KT, Malm G, Ygge J, Engman ML, Maly E, Evengård B. 2000. Ophthalmological findings in children with congenital toxoplasmosis. Report from a Swedish prospective screening study of congenital toxoplasmosis with two years of follow-up. Acta Ophthalmol Scand 78:569–575. https://doi.org/10.1034/j.1600-0420.2000.078005569.x.
4. Ander SE, Rudzki EN, Arora N, Sadovsky Y, Coyne CB, Boyle JP. 2018. Human placental syncytiotrophoblasts restrict *Toxoplasma gondii* attachment and replication and respond to infection by producing immunomodulatory chemokines. mBio 9:e01678-17. https://doi.org/10.1128/mBio.01678-17.
5. Klarquist J, Tobin K, Farhangi Oskuei P, Henning SW, Fernandez MF, Dellacecca ER, Navarro FC, Eby JM, Chatterjee S, Mehrotra S, Clark JI, Le Poole IC. 2016. Ccl22 diverts T regulatory cells and controls the growth of melanoma. Cancer Res 76:6230–6240. https://doi.org/10.1158/0008-5472.CAN-16-0618.
6. Layseca-Espinosa E, Korniotis S, Montandon R, Gras C, Bouillié M, Gonzalez-Amaro R, Dy M, Zavala F. 2013. CCL22-producing CD8α^- myeloid dendritic cells mediate regulatory T cell recruitment in response to G-CSF treatment. J Immunol 191:2266–2272. https://doi.org/10.4049/jimmunol.1202307.
7. Freier CP, Kuhn C, Rapp M, Endres S, Mayr D, Friese K, Anz D, Jeschke U. 2015. Expression of CCL22 and infiltration by regulatory T cells are increased in the decidua of human miscarriage placentas. Am J Reprod Immunol 74:216–227. https://doi.org/10.1111/aji.12399.
8. Martinez de la Torre Y, Buracchi C, Borroni EM, Dupor J, Bonecchi R, Nebuloni M, Pasqualini F, Doni A, Lauri E, Agostinis C, Bulla R, Cook DN, Haribabu B, Meroni P, Rukavina D, Vago L, Tedesco F, Vecchi A, Lira SA, Locati M, Mantovani A. 2007. Protection against inflammation- and autoantibody-caused fetal loss by the chemokine decoy receptor D6. Proc Natl Acad Sci U S A 104:2319–2324. https://doi.org/10.1073/pnas.0607514104.
9. Martinenaite E, Munir Ahmad S, Hansen M, Met Ö, Westergaard MW, Larsen SK, Klausen TW, Donia M, Svane IM, Andersen MH. 2016. CCL22-specific T cells: modulating the immunosuppressive tumor microenvironment. Oncoimmunology 5:e1238541. https://doi.org/10.1080/2162402X.2016.1238541.
10. Kimura S, Tanimoto A, Wang K-Y, Shimajiri S, Guo X, Tasaki T, Yamada S, Sasaguri Y. 2012. Expression of macrophage-derived chemokine (CCL22) in atherosclerosis and regulation by histamine via the H2 receptor. Pathol Int 62:675–683. https://doi.org/10.1111/j.1440-1827.2012.02854.x.
11. Ryning FW, Remington JS. 1978. Effect of cytochalasin D on *Toxoplasma gondii* cell entry. Infect Immun 20:739–743. https://doi.org/10.1128/iai.20.3.739-743.1978.
12. Li L, Li X, Yan J. 2008. Alterations of concentrations of calcium and arachidonic acid and agglutinations of microfilaments in host cells during *Toxoplasma gondii* invasion. Vet Parasitol 157:21–33. https://doi.org/10.1016/j.vetpar.2008.07.007.
13. Franco M, Panas MW, Marino ND, Lee M-CW, Buchholz KR, Kelly FD, Bednarski JJ, Sleckman BP, Pourmand N, Boothroyd JC. 2016. A novel secreted protein, MYR1, is central to *Toxoplasma*'s manipulation of host cells. mBio 7:e02231-15. https://doi.org/10.1128/mBio.02231-15.
14. Marino ND, Panas MW, Franco M, Theisen TC, Naor A, Rastogi S, Buchholz KR, Lorenzi HA, Boothroyd JC. 2018. Identification of a novel protein complex essential for effector translocation across the parasitophorous vacuole membrane of *Toxoplasma gondii*. PLoS Pathog 14:e1006828. https://doi.org/10.1371/journal.ppat.1006828.
15. Olias P, Etheridge RD, Zhang Y, Holtzman MJ, Sibley LD. 2016. *Toxoplasma* effector recruits the Mi-2/NuRD complex to repress STAT1 transcription and block IFN-γ-dependent gene expression. Cell Host Microbe 20:72–82. https://doi.org/10.1016/j.chom.2016.06.006.
16. Braun L, Brenier-Pinchart M-P, Yogavel M, Curt-Varesano A, Curt-Bertini R-L, Hussain T, Kieffer-Jaquinod S, Coute Y, Pelloux H, Tardieux I, Sharma A, Belrhali H, Bougdour A, Hakimi M-A. 2013. A *Toxoplasma* dense granule protein, GRA24, modulates the early immune response to infection by promoting a direct and sustained host p38 MAPK activation. J Exp Med 210:2071–2086. https://doi.org/10.1084/jem.20130103.

17. Shastri AJ, Marino ND, Franco M, Lodoen MB, Boothroyd JC. 2014. GRA25 is a novel virulence factor of *Toxoplasma gondii* and influences the host immune response. Infect Immun 82:2595–2605. https://doi.org/10.1128/IAI.01339-13.
18. He H, Brenier-Pinchart M-P, Braun L, Kraut A, Touquet B, Couté Y, Tardieux I, Hakimi M-A, Bougdour A. 2018. Characterization of a *Toxoplasma* effector uncovers an alternative GSK3/β-catenin-regulatory pathway of inflammation. Elife 7:e39887. https://doi.org/10.7554/eLife.39887.
19. Lodoen MB, Gerke C, Boothroyd JC. 2010. A highly sensitive FRET-based approach reveals secretion of the actin-binding protein toxofilin during *Toxoplasma gondii* infection. Cell Microbiol 12:55–66. https://doi.org/10.1111/j.1462-5822.2009.01378.x.
20. Delorme-Walker V, Abrivard M, Lagal V, Anderson K, Perazzi A, Gonzalez V, Page C, Chauvet J, Ochoa W, Volkmann N, Hanein D, Tardieux I. 2012. Toxofilin upregulates the host cortical actin cytoskeleton dynamics, facilitating *Toxoplasma* invasion. J Cell Sci 125:4333–4342. https://doi.org/10.1242/jcs.103648.
21. Riezu-Boj J-I, Larrea E, Aldabe R, Guembe L, Casares N, Galeano E, Echeverria I, Sarobe P, Herrero I, Sangro B, Prieto J, Lasarte J-J. 2011. Hepatitis C virus induces the expression of CCL17 and CCL22 chemokines that attract regulatory T cells to the site of infection. J Hepatol 54:422–431. https://doi.org/10.1016/j.jhep.2010.07.014.
22. Jeong S-I, Choi B-M, Jang SI. 2010. Sulforaphane suppresses TARC/CCL17 and MDC/CCL22 expression through heme oxygenase-1 and NF-κB in human keratinocytes. Arch Pharm Res 33:1867–1876. https://doi.org/10.1007/s12272-010-1120-6.
23. Wiley M, Teygong C, Phelps E, Radke J, Blader IJ. 2011. Serum response factor regulates immediate early host gene expression in *Toxoplasma gondii*-infected host cells. PLoS One 6:e18335. https://doi.org/10.1371/journal.pone.0018335.
24. Saeij JPJ, Coller S, Boyle JP, Jerome ME, White MW, Boothroyd JC. 2007. *Toxoplasma* co-opts host gene expression by injection of a polymorphic kinase homologue. Nature 445:324–327. https://doi.org/10.1038/nature05395.
25. Nadipuram SM, Kim EW, Vashisht AA, Lin AH, Bell HN, Coppens I, Wohlschlegel JA, Bradley PJ. 2016. *In vivo* biotinylation of the *Toxoplasma* parasitophorous vacuole reveals novel dense granule proteins important for parasite growth and pathogenesis. mBio 7:e00808-16. . https://doi.org/10.1128/mBio.00808-16. [PMC].
26. English ED, Adomako-Ankomah Y, Boyle JP. 2015. Secreted effectors in *Toxoplasma gondii* and related species: determinants of host range and pathogenesis? Parasite Immunol 37:127–140. https://doi.org/10.1111/pim.12166.
27. Blank ML, Parker ML, Ramaswamy R, Powell CJ, English ED, Adomako-Ankomah Y, Pernas LF, Workman SD, Boothroyd JC, Boulanger MJ, Boyle JP. 2018. A *Toxoplasma gondii* locus required for the direct manipulation of host mitochondria has maintained multiple ancestral functions. Mol Microbiol 108:519–535. https://doi.org/10.1111/mmi.13947.
28. English ED, Boyle JP. 2018. Impact of engineered expression of mitochondrial association factor 1b on *Toxoplasma gondii* infection and the host response in a mouse model. mSphere 3:e00471-18. https://doi.org/10.1128/mSphere.00471-18.
29. Hakimi M-A, Olias P, Sibley LD. 2017. *Toxoplasma* effectors targeting host signaling and transcription. Clin Microbiol Rev 30:615–645. https://doi.org/10.1128/CMR.00005-17.
30. Lee CW, Sukhumavasi W, Denkers EY. 2007. Phosphoinositide-3-kinase-dependent, MyD88-independent induction of CC-type chemokines characterizes the macrophage response to *Toxoplasma gondii* strains with high virulence. Infect Immun 75:5788–5797. https://doi.org/10.1128/IAI.00821-07.
31. Hill RD, Gouffon JS, Saxton AM, Su C. 2012. Differential gene expression in mice infected with distinct *Toxoplasma* strains. Infect Immun 80:968–974. https://doi.org/10.1128/IAI.05421-11.
32. Jensen KDC, Wang Y, Wojno EDT, Shastri AJ, Hu K, Cornel L, Boedec E, Ong Y-C, Chien Y, Hunter CA, Boothroyd JC, Saeij JPJ. 2011. *Toxoplasma* polymorphic effectors determine macrophage polarization and intestinal inflammation. Cell Host Microbe 9:472–483. https://doi.org/10.1016/j.chom.2011.04.015.
33. Rosowski EE, Lu D, Julien L, Rodda L, Gaiser RA, Jensen KDC, Saeij JPJ. 2011. Strain-specific activation of the NF-kappaB pathway by GRA15, a novel *Toxoplasma gondii* dense granule protein. J Exp Med 208:195–212. https://doi.org/10.1084/jem.20100717.
34. Lee JW, Zemojtel T, Shakhnovich E. 2009. Systems-level evidence of transcriptional co-regulation of yeast protein complexes. J Comput Biol 16:331–339. https://doi.org/10.1089/cmb.2008.17TT.
35. Rosenberg A, Sibley LD. 2021. *Toxoplasma gondii* secreted effectors co-opt host repressor complexes to inhibit necroptosis. Cell Host Microbe 29:1186–1198. https://doi.org/10.1016/j.chom.2021.04.016.
36. Ong Y-C, Reese ML, Boothroyd JC. 2010. *Toxoplasma* rhoptry protein 16 (ROP16) subverts host function by direct tyrosine phosphorylation of STAT6. J Biol Chem 285:28731–28740. https://doi.org/10.1074/jbc.M110.112359.
37. Gay G, Braun L, Brenier-Pinchart M-P, Vollaire J, Josserand V, Bertini R-L, Varesano A, Touquet B, De Bock P-J, Coute Y, Tardieux I, Bougdour A, Hakimi M-A. 2016. *Toxoplasma gondii* TgIST co-opts host chromatin repressors dampening STAT1-dependent gene regulation and IFN-γ-mediated host defenses. J Exp Med 213:1779–1798. https://doi.org/10.1084/jem.20160340.
38. Gupta D, Wang Q, Vinson C, Dziarski R. 1999. Bacterial peptidoglycan induces CD14-dependent activation of transcription factors CREB/ATF and AP-1. J Biol Chem 274:14012–14020. https://doi.org/10.1074/jbc.274.20.14012.
39. Hall AJ, Vos HL, Bertina RM. 1999. Lipopolysaccharide induction of tissue factor in THP-1 cells involves Jun protein phosphorylation and nuclear factor kappaB nuclear translocation. J Biol Chem 274:376–383. https://doi.org/10.1074/jbc.274.1.376.
40. Wan J, Shan Y, Fan Y, Fan C, Chen S, Sun J, Zhu L, Qin L, Yu M, Lin Z. 2016. NF-κB inhibition attenuates LPS-induced TLR4 activation in monocyte cells. Mol Med Rep 14:4505–4510. https://doi.org/10.3892/mmr.2016.5825.
41. Carruthers VB, Håkansson S, Giddings OK, Sibley LD. 2000. *Toxoplasma gondii* uses sulfated proteoglycans for substrate and host cell attachment. Infect Immun 68:4005–4011. https://doi.org/10.1128/IAI.68.7.4005-4011.2000.
42. Harper JM, Hoff EF, Carruthers VB. 2004. Multimerization of the *Toxoplasma gondii* MIC2 integrin-like A-domain is required for binding to heparin and human cells. Mol Biochem Parasitol 134:201–212. https://doi.org/10.1016/j.molbiopara.2003.12.001.
43. Konradt C, Ueno N, Christian DA, Delong JH, Pritchard GH, Herz J, Bzik DJ, Koshy AA, McGavern DB, Lodoen MB, Hunter CA. 2016. Endothelial cells are a replicative niche for entry of *Toxoplasma gondii* to the central nervous system. Nat Microbiol 1:16001. https://doi.org/10.1038/nmicrobiol.2016.1.
44. Platt DJ, Smith AM, Arora N, Diamond MS, Coyne CB, Miner JJ. 2018. Zika virus-related neurotropic flaviviruses infect human placental explants and cause fetal demise in mice. Sci Transl Med 10:eaao7090. https://doi.org/10.1126/scitranslmed.aao7090.
45. Dubey JP, Tilahun G, Boyle JP, Schares G, Verma SK, Ferreira LR, Oliveira S, Tiao N, Darrington C, Gebreyes WA. 2013. Molecular and biological characterization of first isolates of *Hammondia hammondi* from cats from Ethiopia. J Parasitol 99:614–618. https://doi.org/10.1645/12-51.1.
46. Dubey JP, Sreekumar C. 2003. Redescription of *Hammondia hammondi* and its differentiation from *Toxoplasma gondii*. Int J Parasitol 33:1437–1453. https://doi.org/10.1645/12-51.1.
47. Sokol SL, Primack AS, Nair SC, Wong ZS, Tembo M, Verma SK, Cerqueira-Cezar CK, Dubey JP, Boyle JP. 2018. Dissection of the *in vitro* developmental program of *Hammondia hammondi* reveals a link between stress sensitivity and life cycle flexibility in *Toxoplasma gondii*. Elife 7:e36491. https://doi.org/10.7554/eLife.36491.
48. Barrett T, Wilhite SE, Ledoux P, Evangelista C, Kim IF, Tomashevsky M, Marshall KA, Phillippy KH, Sherman PM, Holko M, Yefanov A, Lee H, Zhang N, Robertson CL, Serova N, Davis S, Soboleva A. 2013. NCBI GEO: archive for functional genomics data sets—update. Nucleic Acids Res 41:D991–D995. https://doi.org/10.1093/nar/gks1193.
49. Gautier L, Cope L, Bolstad BM, Irizarry RA. 2004. affy—analysis of Affymetrix GeneChip data at the probe level. Bioinformatics 20:307–315. https://doi.org/10.1093/bioinformatics/btg405.
50. Grabherr MG, Haas BJ, Yassour M, Levin JZ, Thompson DA, Amit I, Adiconis X, Fan L, Raychowdhury R, Zeng Q, Chen Z, Mauceli E, Hacohen N, Gnirke A, Rhind N, di Palma F, Birren BW, Nusbaum C, Lindblad-Toh K, Friedman N, Regev A. 2011. Full-length transcriptome assembly from RNA-Seq data without a reference genome. Nat Biotechnol 29:644–652. https://doi.org/10.1038/nbt.1883.
51. Smith AF, Posakony JW, Rebeiz M. 2017. Automated tools for comparative sequence analysis of genic regions using the GenePalette application. Dev Biol 429:158–164. https://doi.org/10.1016/j.ydbio.2017.06.033.
52. Shen B, Brown KM, Lee TD, Sibley LD. 2014. Efficient gene disruption in diverse strains of *Toxoplasma gondii* using CRISPR/CAS9. mBio 5:e01114-14. https://doi.org/10.1128/mBio.01114-14.
53. Saeij JPJ, Boyle JP, Coller S, Taylor S, Sibley LD, Brooke-Powell ET, Ajioka JW, Boothroyd JC. 2006. Polymorphic secreted kinases are key virulence factors in toxoplasmosis. Science 314:1780–1783. https://doi.org/10.1126/science.1133690.

54. Coombs RS, Blank ML, English ED, Adomako-Ankomah Y, Urama I-CS, Martin AT, Yarovinsky F, Boyle JP. 2020. Immediate interferon gamma induction determines murine host compatibility differences between *Toxoplasma gondii* and *Neospora caninum*. Infect Immun 88:e00027-20. https://doi.org/10.1128/IAI.00027-20.
55. Huynh M-H, Carruthers VB. 2009. Tagging of endogenous genes in a *Toxoplasma gondii* strain lacking Ku80. Eukaryot Cell 8:530–539. https://doi.org/10.1128/EC.00358-08.
56. Love MI, Huber W, Anders S. 2014. Moderated estimation of fold change and dispersion for RNA-seq data with DESeq2. Genome Biol 15:550. https://doi.org/10.1186/s13059-014-0550-8.
57. Croken MM, Qiu W, White MW, Kim K. 2014. Gene set enrichment analysis (GSEA) of *Toxoplasma gondii* expression datasets links cell cycle progression and the bradyzoite developmental program. BMC Genomics 15:515. https://doi.org/10.1186/1471-2164-15-515.
58. Krämer A, Green J, Pollard J, Tugendreich S. 2014. Causal analysis approaches in Ingenuity pathway analysis. Bioinformatics 30:523–530. https://doi.org/10.1093/bioinformatics/btt703.
59. Saeij JPJ, Boyle JP, Grigg ME, Arrizabalaga G, Boothroyd JC. 2005. Bioluminescence imaging of *Toxoplasma gondii* infection in living mice reveals dramatic differences between strains. Infect Immun 73:695–702. https://doi.org/10.1128/IAI.73.2.695-702.2005.